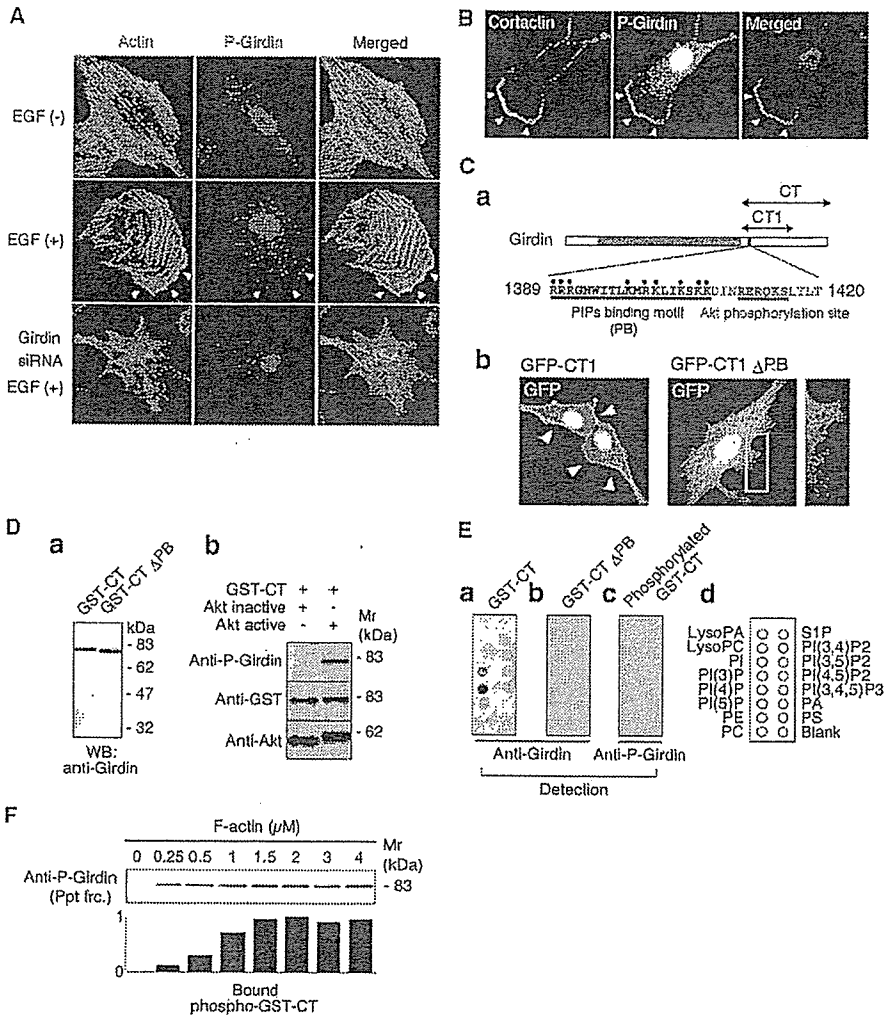

Figure 6. Effects of Girdin Phosphorylation on Its Localization and Interaction with Phosphoinositides

(A) Quiescent (upper panel), EGF (50 ng/ml)-stimulated (middle panel), and Girdin siRNA-transfected (lower panel) Vero cells were fixed and stained with Alexa488-phalloidin and anti-phospho Girdin (P-Girdin) antibody. Arrows denote the lamellipodia where the phosphorylated Girdin accumulates.

(B) Migrating Vero cells were stained with anti-Cortactin and anti-P-Girdin antibody.

(C) (Ca) The putative phosphoinositide binding site (PB) upstream of the Akt phosphorylation site in Girdin is indicated. (Cb) Vero cells were transfected with either GFP-CT1 (left) or GFP-CT1 in which the phosphoinositide binding site was deleted (GFP-CT1 ΔPB) (right). Arrows denote GFP signals at the plasma membrane.

(D) Purification of GST-CT and protein-lipid overlay assays. (Da) Purified GST-CT and GST-CT ΔPB were analyzed by Western blotting with anti-Girdin antibody. (Db) Phosphorylation of purified GST-CT by recombinant Akt in vitro. The phosphorylated GST-CT in an in vitro kinase assay was detected with anti-P-Girdin antibody.

(E) Protein-lipid overlay assays with (Ea) GST-CT, (Eb) GST-CT ΔPB, and the (Ec) phosphorylated GST-CT. The lipid binding of both GST-CT and GST-CT ΔPB was detected with anti-Girdin antibody, whereas that of phosphorylated GST-CT was detected with anti-P-Girdin antibody. (Ed) The various lipids spotted on the membrane (100 pmol lipid per spot) are indicated. PA, phosphatidic acid; PC, phosphocholine; PI, phosphatidylinositol; PE, phosphatidylethanolamine; PS, phosphatidylserine; S1P, sphingosine-1-phosphate.

(F) Binding of phosphorylated Girdin CT to F-actin. GST-CT was phosphorylated by Akt in vitro (Db) and subjected to an actin cosedimentation assay. A fixed amount of GST-CT (1 μM) was phosphorylated in vitro and mixed with various amount of F-actin (0–4 μM), followed by ultracentrifugation. The amount of phosphorylated GST-CT bound to F-actin in the pellet fraction (Ppt frc.) was monitored by Western blot analyses with anti-P-Girdin antibody.

notion that the interaction of endogenous Girdin with actin filaments is important for integral cell migration. Consistent with previous studies (Higuchi et al., 2001; Kim et al., 2001), the depletion of Akt by siRNA also attenuated the migration (Figure 7B), which suggests that intrinsic Akt activity is requisite for Vero cells to migrate through the pores in this assay system.

To next examine whether adding Girdin exogenously

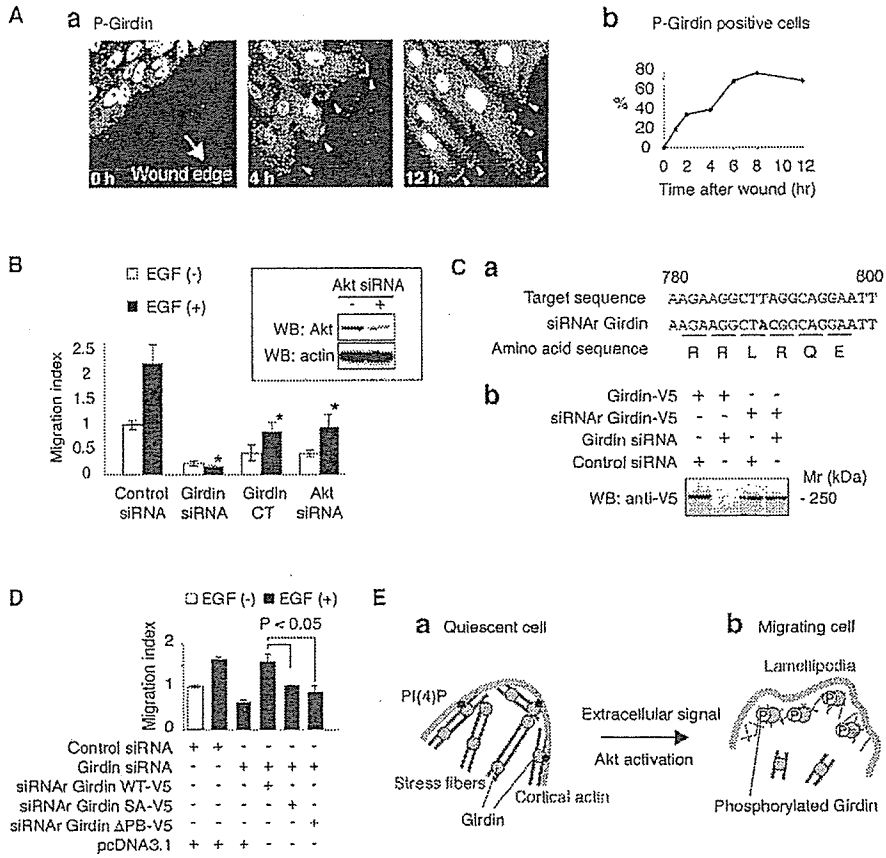

Figure 7. Phosphorylation of Girdin Regulates Cell Migration

(A) Girdin is phosphorylated at the leading edge during cell migration. (Aa) After scratching a monolayer of Vero cells, the cells facing the wound were fixed and stained with anti-P-Girdin antibody. Arrowheads denote the signals of the phosphorylated Girdin. (Ab) The phosphorylation of Girdin localizing at the leading edge increases in a time-dependent fashion.

(B) Vero cells were transfected with GFP (0.5 μg) and either siRNA (20 pmol) or Girdin CT (2.5 μg), incubated for 48 hr, and subjected to Boyden chamber assays in the presence or absence of EGF (100 ng/ml) in the lower chamber. Asterisks indicate statistical significance (Student's t test; *p < 0.05) compared with control. The inset shows the depletion of Akt in Vero cells by siRNA. The results represent the mean ± SE.

(C) Generation of an siRNA-resistant (siRNAr) mutant of Girdin. (Ca) The target sequence of Girdin siRNA ("B" in Figure 4A) and the nucleotide substitution for the generation of the siRNAr version are indicated. (Cb) Cell lysates from COS7 cells cotransfected with indicated siRNAs and constructs were analyzed by Western blotting with anti-V5 antibody.

(D) Vero cells were cotransfected with GFP (0.5 μg), siRNAs (20 pmol), and indicated constructs (2.5 μg), incubated for 48 hr, and subjected to Boyden chamber assays. Expression levels of Girdin mutants in cells prior to plating for migration assays were monitored by Western blot analysis with anti-V5 antibody and were found to be similar (data not shown). The results represent the mean ± SE.

(E) A proposed model for the regulation of cell motility by the phosphorylation of Girdin. In (Ea) quiescent cells, Girdin crosslinks actin filaments and anchors cortical actin at the plasma membrane, whereas during (Eb) cell migration, Akt-mediated phosphorylation allows Girdin to localize at the leading edge and contribute to the formation of short-branched filaments in the lamellipodium.

restores the defect in cell migration observed in the knockdown cells, we constructed siRNA-resistant (siRNAr) versions of Girdin harboring silent mutations (Figure 7C). As shown in Figure 7D, the expression of the siRNAr-Girdin WT fully restored migratory response to EGF. In contrast, the expression of the siRNAr-Girdin mutants in which the Ser-1416 was mutated to Ala (siRNAr-Girdin SA), the phosphoinositide binding site was deleted (siRNAr-Girdin ΔPB), or the basic residues in the phosphoinositide binding site were replaced with alanines (siRNAr-Girdin PBala) failed to complement the migration defect (Figure 7D and Figure S5C). We also confirmed these findings by performing migration assays with a human fibrosarcoma cell line, HT-1080 (Figure S7).

Finally, we directly examined the movement of Vero cells expressing the Girdin mutants by wound-healing assays (Figure S8 and Movies S3–S6). Cells expressing Girdin WT effectively and rapidly moved into the wound (Movie S3), but those expressing Girdin SA exhibited elongated shape. Moreover, the location of the nuclei of the latter cells seemed to be fixed and motionless, suggesting that the cells could not undergo detachment from the matrix (Movie S4). Cells expressing Gir-

din ΔPB and Girdin PBala were less locomotive compared with those expressing Girdin WT (Movies S5 and S6, respectively). These results demonstrate that expression of the Girdin mutants impairs proper directional cell migration. Considered with the findings shown in Figure 6 and Figure S6, these data indicate that the regulation of an interaction between Girdin and the plasma membrane by Akt is crucial for cell migration.

Discussion

The Structure of Girdin/APE and Its Roles in Actin Organization

In a search for molecules that interact with Akt, we have identified a novel, to our knowledge, actin binding protein, designated Girdin/APE, that is essential for actin organization. Four different regions can be distinguished in the Girdin molecule based on the sequences of its subunits, subcellular localization, and functions: an N-terminal region that seems to facilitate the formation of a dimer (NT), an extremely long coiled-coil region, a region that binds to the plasma membrane through the interaction with phosphoinositides (CT1), and a C-terminal region that encompasses an actin binding site (CT2). The amino acid sequence of the CT2 domain shows no homology with the calponin homology (CH) domain, a common actin binding domain that is present in most actin binding proteins such as α-actinin, filamins, fimbrin, spectrins, cortexillins, and dystrophin (Gimona et al., 2002), suggesting that Girdin represents a novel class of actin binding proteins.

Analysis of the sequence of Girdin reveals that it includes 135 heptad repeats, $(abcdefg)_{135}$, between Leu-253 and Lys-1375 that correspond to a central rod domain. Within the repeats, positions *a* and *d* are preferentially occupied by hydrophobic residues like Leu, Ile, Met, or Val (Figure S1), which is consistent with the signature of canonical coiled-coil structures that wind around each other in a superhelix (Cohen and Parry, 1994). The oligomerization properties of coiled-coil sequences are determined by the distribution of β-branched residues in the *a* or *d* positions (Harbury et al., 1993; Faix et al., 1996). Val and Ile in *a* favor dimerization, they favor tetramerization in *d*, and their presence in both *a* and *d* facilitates the formation of trimers. In the coiled-coil sequence of Girdin, 22 repeats have Val or Ile in the *a* position, whereas they are present in the *d* position of only 9 repeats, suggesting that the coiled-coil domain of Girdin tends to form a dimer. This is consistent with our findings suggested by gel filtration that the NT domain of Girdin forms a dimer (Figure S2).

It has been established that the possession of two actin binding sites enables crosslinking or bundling proteins to link filaments and to stabilize higher-order assemblies of actin filaments (Pollard, 2002). Possessing two actin binding CT2 domains in juxtaposition, the dimeric Girdin molecules seem to be designed to gather actin filaments together into bundles or a meshwork. Consistent with this possibility are the findings of immunofluorescent staining and electron microscopy that the depletion of Girdin interfered with actin networks, leading to the disruption of stress fibers, cortical actin filaments, and actin meshwork at the leading edge. During migration, the Girdin knockdown cells produced multiple protrusions, resulting in limited directional migration. These observations indicate that Girdin fulfils an essential function in determining the stability and integrity of actin bundles and meshwork that mediates a variety of important biological processes. Eukaryotic cells have a fail-safe mechanism in the multiple actin crosslinking proteins that share overlapping functions (Pollard, 2002). The phenotypic consequences of the depletion of Girdin indicate that the presence of other proteins cannot completely compensate for its loss. Because the speculated primary structure, molecular size, and putative function of Girdin are reminiscent of those of filamin (Stossel et al., 2001), it is important to clarify the functional difference and synergism between the two.

We found that the CT1 domain of Girdin associates with the plasma membrane through the cluster of basic amino acid residues Arg-1389 to Lys-1407. This positively charged sequence is related to a consensus sequence for PI(4,5)P2 binding, which has been found in gelsolin, villin, profilin, vinculin, and other various cytoskeletal proteins (Janmey et al., 1992). Unexpectedly, our experiment showed that the basic amino acid cluster in Girdin does not bind to PI(4,5)P2, but binds to PI(4)P and binds weakly to PI(3)P. Considering that PI(4)P, but not PI(3)P, is abundant in mammalian cells (Vanhaesebroeck et al., 2001), it is plausible to conclude that Girdin binds to PI(4)P, which resides in the membranes of mammalian cells in an amount equal to that of PI(4,5)P2. We speculate that it stabilizes the cortical actin filaments by anchoring them at the plasma membrane.

Roles of Girdin and Its Regulation in Cell Motility

Relatively little is known about how cells regulate actin crosslinking proteins in response to external stimuli (Pollard, 2002; Small et al., 2002). In the present study, we found that Akt phosphorylates Girdin in vitro and in intact cells. The phosphorylation of Girdin was induced by EGF and during cell migration, suggesting a significance for phosphorylation in physiological cellular events. In migrating Vero fibroblasts, the phosphorylated Girdin preferentially localizes to lamellipodia at the leading edge, which is in line with our and previous observations that activated Akt is also localized at the leading edge during migration in mammalian cells (Higuchi et al., 2001; Kim et al., 2001; Figure S4). It is plausible that Akt, activated downstream of PI3K, translocates from the cytosol to the leading edge through its PH domain, and subsequently phosphorylates Girdin on the actin filaments at the front of the cells.

How does Akt regulate the function of Girdin by phosphorylation? Insight into this issue comes from our observation that the phosphorylation of the CT domain of Girdin affects in vitro binding to PI(4)P. Because the phosphorylation site is present in the neighborhood of the phosphoinositide binding site, it is speculated that phosphorylation induces a conformational change around these sites, and this change in turn alters affinity for the phosphoinositide. We further found that the phosphorylated CT domain retains the property of actin

binding, and its affinity for F-actin is comparable to that of the nonphosphorylated form. Based on these observations, we speculate that phosphorylation by Akt releases Girdin from PI(4)P and allows it to localize at the leading edge in order to crosslink the newly generated actin filaments in the lamellipodium network, as illustrated in Figure 7E.

The leading lamellipodium of motile cells is a sheet-like protrusion filled with actin filaments at high density (Small et al., 2002). Because long and flexible actin filaments cannot sustain a pushing force (Pollard and Borisy, 2003), cells must create a dense array of short-branched filaments by utilizing crosslinking proteins, which allow nascent filaments to push against the membrane at the leading edge. The major crosslinking components at lamellipodium are filamin and α-actinin (Small et al., 2002). Cells derived from human malignant melanomas lacking filamin had unstable lamellipodia and exhibited impaired locomotion (Stossel et al., 2001). *Dictyostelium* cells lacking both α-actinin and ABP-120 (the filamin homolog) showed motility defects (Rivero et al., 1996). Both of these proteins have a relatively low affinity for actin filaments, with K_d values in the micromolar range. This low affinity enables their rapid binding and dissociation with the filaments and allows networks of actin filaments to passively change shape when prolonged force is applied while resisting rapid deformations (Pollard, 2002). This is also the case with Girdin, which has a low affinity for F-actin, with a K_d value of ~1 μM. An important goal is to reveal functional divergence and structural complementation between Girdin and other crosslinking proteins in the lamellipodium.

The role of Girdin in cell migration is supported by the findings that Girdin knockdown cells migrated poorly and exhibited insufficient lamellipodium formation at their leading edge. However, they revert to normal behavior when siRNAr-Girdin is added. In contrast, cells expressing siRNAr-Girdin SA, ΔPB, and PBala mutants exhibited limited migration (Figure 7, Figure S8, and Movies S3–S6). As Girdin SA may be constantly anchored at the plasma membrane without undergoing phosphorylation, and Girdin ΔPB and PBala do not associate with the plasma membrane (Figure S6), our findings suggest that spatially selective regulation of Girdin phosphorylation by Akt at the cytoplasm-membrane interface is essential for reorganization of the actin cytoskeleton.

Activation of Akt is correlated with an increase in cell migration and invasion in several mammalian systems. The overexpression of active Akt promotes cell motility in mammalian cells such as fibroblasts, fibrosarcoma cells, and vascular endothelial cells (Higuchi et al., 2001; Kim et al., 2001; Morales-Ruiz et al., 2000). Rac and Cdc42, small GTPases essential for lamellipodia formation and establishment of cell polarity, activate Akt at the leading edge of fibroblasts (Higuchi et al., 2001). Akt is involved in the trafficking and recycling of vitronectin and fibronectin receptors (αvβ3 and α5β1 integrins, respectively), which regulate cell spreading and migration (Roberts et al., 2004). Finally, the association of Pak1 (p21-activated protein kinase) with Nck, an adaptor protein, is crucial for cell movement and is modulated by Akt (Zhou et al., 2003). Along with our present findings, these data indicate the involvement of Akt in cell motility. In addition, it was recently demonstrated that Akt and its substrate glycogen synthase kinase-3β (GSK-3β) are essential proteins in the determination of axon-dendrite polarity of neurons (Yoshimura et al., 2005; Jiang et al., 2005). Because the depletion of Girdin results in the formation of multiple leading edges and limited directional migration in Vero fibroblasts, the possible involvement of the Akt-Girdin pathway in the regulation of cell polarity should not be overlooked.

In conclusion, we demonstrated a novel, to our knowledge, role of Girdin/APE in actin organization and cell motility that is regulated by Akt. Anai et al. (2005) reported that Girdin/APE also functions as an enhancer of Akt and stimulates DNA synthesis. When Girdin/APE and Akt were overexpressed in cells, they found that cell proliferation was inhibited and apoptosis was induced. Thus, further investigation could shed light on important roles of Girdin/APE in different cellular processes.

Experimental Procedures

Yeast Two-Hybrid Assays

To identify proteins interacting with Akt, a full-length cDNA encoding human Akt1 was inserted into the pAS2 vector (Clontech). The resulting construct was used as bait to screen a human fetal brain MATCHMAKER cDNA library as previously described (Murakami et al., 2002). Two positive plasmids containing cDNA inserts were selected and sequenced. They contained the cDNA fragments encoding the C-terminal region of Girdin (residues 1217–1870). A full-length cDNA encoding Girdin was isolated from the human fetal brain poly A$^+$ RNA by 5′ rapid amplification of cDNA ends (5′-RACE system, Invitrogen). Additionally, we performed yeast two-hybrid binding assays with purified pAS and pACT constructs containing the fragments of human Akt1 and Girdin cDNAs.

Plasmids

Wild-type, constitutively active, and dominant-negative human Akt1 constructs were generously provided by Y. Gotoh (University of Tokyo). The constructs of pcDNA3.1-, pGEX-, and pEGFP-Girdin fragments were produced as described elsewhere (Murakami et al., 2002). EGFP was fused to the amino termini, and V5 and myc tags were fused to the carboxyl termini of the proteins. Girdin mutants were generated by using the QuikChange site-directed mutagenesis kit (Stratagene) according to the manufacturer's protocol. The siRNA-resistant Girdin was created by introducing two silent mutations into Girdin at nucleotides 780–800 (5′-AAGAAGGCTACGG CAGGAATT-3′) (underline indicates mutations).

Antibodies

Rabbit anti-Girdin polyclonal antibody was developed against the 19 carboxyl-terminal amino acids of Girdin and affinity-purified with the immunized peptide. The anti-phospho Girdin polyclonal antibody was supplied by Kumamoto Immunochemical Laboratory, Transgenic, Inc. (Kumamoto, Japan). It was raised by immunizing rabbits with a keyhole limpet hemocyanin-conjugated phosphopeptide corresponding to Girdin amino acid sequence 1408–1420 (CDINRERQKpSLTLT). Antiserum was purified as a bound fraction of the phosphopeptide-conjugated column.

Other antibodies used in this study include anti-Akt polyclonal antibody (Cell Signaling Technology), anti-phospho Akt polyclonal antibody (Cell Signaling Technology), and anti-Cortactin monoclonal antibody (Upstate).

Kinase Assays

Immunoprecipitates with anti-V5 antibody (Invitrogen) from COS7 cells expressing Girdin CT-V5 WT or SA or purified GST-CT were incubated with recombinant active or inactive Akt (500 ng) (Up-

state) with 10 μCi [γ-^{32}P]ATP (3000 Ci/mmol, Amersham) in kinase buffer (20 mM MOPS, 25 mM β-glycerophosphate, 5 mM EGTA, 15 mM $MgCl_2$, 1 mM dithiothreitol, and 1 mM $NaVO_3$). Mixtures were incubated at 30°C for 30 min, and reactions were terminated by the addition of Laemmli sodium dodecyl sulfate (SDS) sample dilution buffer (20 mM Tris-HCl [pH 6.8], 2 mM EDTA, 2% SDS, 10% sucrose, 20 μg/ml bromophenol blue, 80 mM dithiothreitol).

Immunofluorescent Staining

Vero cells were plated on fibronectin- (10 μg/ml, Sigma) and collagen I (10 μg/ml, Upstate)-coated coverslips or glass base dishes, fixed, and stained with the indicated antibodies. Fluorescence was examined by using a confocal laser-scanning microscope (Fluoview FV500, Olympus).

Actin Cosedimentation Assays

F-actin cosedimentation assays were performed according to the manufacturer's protocol (Cytoskeleton). Briefly, purified GST fusion proteins, GST alone, and α-actinin (Cytoskeleton) were incubated for 30 min at room temperature with 40 μg pure actin filaments. The final concentration of F-actin was 18 μM. Filaments were subsequently pelleted by centrifugation (100,000 × g) (Beckman). The cosedimented proteins were resolved by SDS-PAGE and detected by either Coomassie Brilliant Blue (CBB) staining or Western blot analyses with anti-GST antibody (Cell Signaling Technology) or anti-phospho Girdin Ab.

For quantitative analyses, a fixed concentration of GST-Girdin CT2 (1 μM) was mixed with increasing amounts of F-actin (0–2.5 μM) in polymerization buffer and incubated at room temperature for 30 min. Proteins were centrifuged as described above, and total pellets and supernatants were loaded separately on SDS-PAGE. Protein bands were detected by CBB staining and scanned and quantified with the software program WinROOF (Mitani Corp., Fukui, Japan).

RNA Interference

The siRNA-mediated knockdown of Girdin and Akt was performed by using previously described methods (Watanabe et al., 2004). The targeted sequences that effectively mediated the silencing of the expression of Girdin are as follows (only sense sequences are shown): 5′-AACCAGGTCATGCTCCAAATT-3′ (nucleotides 145–165, Girdin siRNA [A]) and 5′-AAGAAGGCTTAGGCAGGAATT-3′ (nucleotides 780–800, Girdin siRNA [B]). The 21 nucleotide synthetic duplexes were prepared by Qiagen. The siRNA specific to human Akt1 was purchased from Qiagen. Vero cells were transfected with the siRNAs or a 21 nucleotide irrelevant RNA (Qiagen) as a control, by using lipofectamine 2000 (Invitrogen) according to the manufacturer's protocol.

Freeze-Replica Electron Microscopy of the Cytoplasmic Cell Surface

Electron microscopy for the cytoplasmic surface of the cell membrane was carried out according to previously described methods (Heuser, 1989, 2000; Usukura, 1993). Vero cells cultured on glass coverslips (3 mm in diameter, standard #1 Matsunami, Osaka, Japan) were transfected with siRNAs. Immediately after being unroofed from the apical cell membrane, the cells were fixed for 30 min in 2.5% glutaraldehyde in buffer A (70 mM KCl, 5 mM $MgCl_2$, 3 mM EGTA, 30 mM HEPES buffer adjusted at pH 7.4 with KOH). After being washed with buffer A/distilled water, specimens were quickly frozen with liquid helium by using the rapid-freezing device (Eiko, Tokyo, Japan). Samples were then freeze etched and rotary shadowed with platinum-carbon, in a newly developed freeze etching device (FR9000, HITACHI, Ibaraki, Japan). For immunolabeling of Girdin molecules, the unroofed cells were fixed for 30 min in 4% paraformaldehyde/0.5% glutaraldehyde in buffer A. After being washed three times with buffer B (100 mM NaCl, 30 mM HEPES, 2 mM $CaCl_2$), the samples were quenched and blocked, and then labeled for 1 hr at 37°C with primary and secondary 10 nm gold-conjugated antibodies (Amersham) in buffer B containing 1% BSA. Finally, specimens were rapidly frozen and freeze etched as described above.

Scratch-Induced Cell Migration and Time-Lapse Imaging

Directional cell migration of Vero cells was stimulated in a monolayer by using an in vitro scratch wound assay (Watanabe et al., 2004). Vero cells were seeded on fibronectin-precoated coverslips or 35 mm glass base dishes and were transfected with indicated siRNAs. A total of 48 hr after the transfection, the confluent Vero cells were scratched with a 200 μl disposable plastic pipette tip and were allowed to migrate toward the wound. The cells were fixed at the indicated times for immunofluorescent staining. For time-lapse observation, cells were cotransfected with siRNAs and GFP-actin and were subjected to the scratch wound assays. The cells at the wound edges were observed with a confocal laser scanning microscope (Fluoview FV500, Olympus).

Three-Dimensional Cell Migration Assays

To assess the motility of cells transfected with various constructs or siRNAs, we performed the modified Boyden chamber migration assay, which enabled us to count GFP-labeled cells migrating across a fluorescence-blocking planer micropore membrane by using HTS FluoroBlok Insert (8.0 μm pores, 24-well format, Becton Dickinson). Both sides of the membrane were coated with 10 μg/ml fibronectin for 12 hr at 37°C and were washed with phosphate-buffered saline (PBS). The chambers were then placed in 24-well dishes filled with Dulbecco's modified Eagle's medium (DMEM) containing 0.1% BSA with or without 20 ng/ml human recombinant EGF. For migration assays of HT-1080 cells, DMEM with 10% fetal bovine serum (FBS) was added to the lower chamber. Cells (1×10^5) were transfected with GFP (0.5 μg, to identify transfected cells), indicated constructs (2.5 μg), and siRNAs (20 pmol) in 24-well plates, plated in the upper compartment, and allowed to migrate through the pores of the membrane for 4 hr. Cell motility was quantified by using a fluorescence microscope to count the GFP-positive cells that had migrated through the membrane.

Protein-Lipid Overlay Assays

GST fusion proteins were expressed in DH5α or BL21-CodonPlus (Stratagene) cells and purified by using conventional methods. Binding of the purified GST-CT to phospholipids was examined at 4°C by using a PIP-Strip (Echelon Bioscience) according to the manufacturer's protocol. Bound GST-CT proteins were detected with either anti-Girdin or anti-phospho Girdin antibodies.

Data Analysis

Data are presented as the mean ± SE. Statistical significance was evaluated by Student's t test.

Supplemental Data

Supplemental Data including eight figures, six movies, and Supplemental Experimental Procedures are available at http://www.developmentalcell.com/cgi/content/full/9/3/389/DC1/.

Acknowledgments

We thank Y. Gotoh (University of Tokyo) for providing Akt cDNAs and helpful discussion, T. Fukuda (Tohoku University) for helpful discussion, M. Nakayama (Nagoya University) for discussions on migration assays, K. Kadomatsu and K. Ichihara (Nagoya University) for providing HT-1080 cells, and N. Saka and A. Muraki (Nagoya University) for help in characterization of Girdin. This work was supported by Grants-in-Aid for Center of Excellence (COE) Research, Scientific Research (A), and Scientific Research on Priority Area "Cancer" from the Ministry of Education, Culture, Sports, Science and Technology of Japan (to M.T.). A.E. is a fellow of the Japan Society for the Promotion of Science.

Received: February 16, 2005
Revised: May 19, 2005
Accepted: August 3, 2005
Published: September 6, 2005

References

Alessi, D.R., Caudwell, F.B., Andjelkovic, M., Hemmings, B.A., and Cohen, P. (1996). Molecular basis for the substrates specificity of

protein kinase B; comparison with MAPKAP kinase-1 and p70 S6 kinase. FEBS Lett. *399*, 333–338.

Anai, M., Shojima, N., Katagiri, H., Ogihara, T., Sakoda, H., Onishi, Y., Ono, H., Fujishiro, M., Fukushima, Y., Horike, N., et al. (2005). A novel protein kinase B (PKB)/AKT-binding protein enhances PKB kinase activity and regulates DNA synthesis. J. Biol. Chem. *280*, 18525–18535.

Brazil, D.P., Park, J., and Hemmings, B.A. (2002). PKB binding proteins: getting in on the Akt. Cell *111*, 293–303.

Chung, Y., Potikyan, G., and Firtel, R.A. (2001). Control of cell polarity and chemotaxis by Akt/PKB and PI3 kinase through the regulation of PAKa. Mol. Cell *7*, 937–947.

Cohen, C., and Parry, D.A.D. (1994). α-helical coiled-coils: more facts and better prediction. Science *265*, 488–489.

Datta, S.R., Brunet, A., and Greenberg, M.E. (1999). Cellular survival: a play in three Akts. Genes Dev. *13*, 2905–2927.

Etienne-Manneville, S., and Hall, A. (2002). Rho GTPases in cell biology. Nature *420*, 629–635.

Faix, J., Steinmetz, M., Boves, H., Kammerer, R.A., Lottspeich, F., Mintert, U., Murphy, J., Stock, A., Aebi, U., and Gerisch, G. (1996). Cortexillins, major determinants of cell shape and size, are actin-bundling proteins with a parallel coiled-coil tail. Cell *86*, 631–642.

Gimona, M., Djinovic-Carugo, K., Kranewitter, W.J., and Winder, S.J. (2002). Functional plasticity of CH domains. FEBS Lett. *513*, 98–106.

Harbury, P.B., Zhang, T., Kim, P.S., and Alber, T. (1993). A switch between two, three and four stranded coiled-coils in GCN4 leucine zipper mutants. Science *262*, 1401–1407.

Heuser, J. (1989). Effect of cytoplasmic acidification on clathrin lattice morphology. J. Cell Biol. *108*, 401–411.

Heuser, J. (2000). The production of 'cell cortices' for light and electron microscopy. Traffic *1*, 545–552.

Higuchi, M., Masuyama, N., Fukui, Y., Suzuki, A., and Gotoh, Y. (2001). Akt mediates Rac/Cdc42-regulated cell motility in growth factor-stimulated cells and invasive PTEN knockout cells. Curr. Biol. *11*, 1958–1962.

Janmey, P.A., Lamb, J., Allen, P.G., and Matsudaira, P.T. (1992). Phosphoinositide-binding peptides derived from the sequence of gelsolin and villin. J. Biol. Chem. *267*, 11818–11823.

Jiang, H., Guo, W., Liang, X., and Rao, Y. (2005). Both the establishment and the maintenance of neuronal polarity require active mechanism: critical roles of GSK-3β and its upstream regulation. Cell *120*, 123–135.

Kim, D., Kim, S., Koh, H., Yoon, S., Chung, A., Cho, K.S., and Chung, J. (2001). Akt/PKB promotes cancer cell invasion via increased motility and metalloproteinase production. FASEB J. *15*, 1953–1962.

Lauffenburger, D.A., and Horwitz, A.F. (1996). Cell migration: a physically integrated molecular process. Cell *84*, 359–369.

Lupas, A., Van Dyke, M., and Stock, J. (1991). Predicting coiled coils from protein sequence. Science *252*, 1162–1164.

Meili, R., Ellsworth, C., Lee, S., Reddy, T.B., Ma, H., and Firtel, R.A. (1999). Chemoattractant-mediated transient activation and membrane localization of Akt/PKB is required for efficient chemotaxis to camp in *Dictyostelium*. EMBO J. *18*, 2092–2105.

Merlot, S., and Firtel, R.A. (2003). Leading the way: directional sensing through phosphatidylinositol 3-kinase and other signaling pathways. J. Cell Sci. *116*, 3471–3478.

Morales-Ruiz, M., Fulton, D., Sowa, G., Languino, L.R., Fujio, Y., Walsh, K., and Sessa, W.C. (2000). Vascular endothelial growth factor-stimulated actin reorganization and migration of endothelial cells is regulated via the serine/threonine kinase Akt. Circ. Res. *86*, 892–896.

Murakami, H., Yamamura, Y., Shimono, Y., Kawai, K., Kurokawa, K., and Takahashi, M. (2002). Role of Dok1 in cell signaling mediated by Ret tyrosine kinase. J. Biol. Chem. *277*, 32781–32790.

Pollard, T.D. (2002). Actin and actin-binding proteins. In Cell Biology, T.D. Pollard and W.C. Earnshaw, eds. (New York: W.B. Saunders), pp. 557–577.

Pollard, T.D., and Borisy, G.G. (2003). Cellular motility driven by assembly and disassembly of actin filaments. Cell *112*, 453–465.

Revenu, C., Athman, R., Robine, S., and Louvard, D. (2004). The co-workers of actin filaments: from cell structures to signals. Nat. Rev. Mol. Cell Biol. *5*, 1–12.

Ridley, A.J. (2001). Rho GTPases and cell migration. J. Cell Sci. *114*, 2713–2722.

Ridley, A.J., Schwartz, M.A., Burridge, K., Firtel, R.A., Ginsberg, M.H., Borisy, G., Parsons, J.T., and Horwitz, A.R. (2003). Cell migration: integrating signals from front to back. Science *302*, 1704–1709.

Rivero, F., Koppel, B., Peracino, B., Bozzaro, S., Siegert, F., Weijer, C.J., Schleicher, M., Albrecht, R., and Noegel, A.A. (1996). The role of the cortical cytoskeleton: F-actin crosslinking proteins protect against osmotic stress, ensure cell size, cell shape and motility, and contribute to phagocytosis and development. J. Cell Sci. *109*, 2679–2691.

Roberts, M.S., Woods, A.J., Dale, T.C., van der Sluijs, P., and Norman, J.C. (2004). Protein kinase B/Akt acts via glycogen synthase kinase 3 to regulate recycling of αvβ3 and α5β1 integrins. Mol. Cell. Biol. *24*, 1505–1515.

Scheid, M.P., and Woodgett, J.R. (2001). PKB/AKT: functional insights from genetic models. Nat. Rev. Mol. Cell Biol. *2*, 760–768.

Sechi, A.S., and Wehland, J. (2000). The actin cytoskeleton and plasma membrane connection: PtdIns(4,5)P_2 influences cytoskeletal protein activity at the plasma membrane. J. Cell Sci. *113*, 3685–3695.

Servant, G., Weiner, O.D., Herzmark, P., Balla, T., Sedat, J.W., and Bourne, H.R. (2000). Polarization of chemoattractant receptor signaling during neutrophil chemotaxis. Science *287*, 1037–1040.

Small, J.V., Stradal, T., Vignal, E., and Rottner, K. (2002). The lamellipodium: where motility begins. Trends Cell Biol. *12*, 112–120.

Stossel, T.P., Condeelis, J., Cooley, L., Hartwig, J.H., Noegel, A., Schleicher, M., and Shapiro, S.S. (2001). Filamins as integrators of cell mechanics and signaling. Nat. Rev. Mol. Cell Biol. *2*, 138–145.

Takahashi, M. (2001). The GDNF/RET signaling pathway and human disease. Cytokine Growth Factor Rev. *12*, 361–373.

Usukura, J. (1993). Rapid freezing and subsequent preparation methods in retinal cell biology. In Methods in Neurosciences, P.A. Hargrave, ed. (San Diego: Academic Press, Inc.), pp. 37–53.

Vanhaesebroeck, B., Leevers, S.J., Ahmadi, K., Timms, J., Katso, R., Driscoll, P.C., Woscholski, R., Parker, P.J., and Waterfield, M.D. (2001). Synthesis and functions of 3-phosohorylated inositol lipids. Annu. Rev. Biochem. *70*, 535–602.

Vivanco, I., and Sawyers, C.L. (2002). The phosphatidylinositol 3-kinase-Akt pathway in human cancer. Nat. Rev. Cancer *2*, 489–501.

Watanabe, T., Wang, S., Noritake, J., Sato, K., Fukata, M., Takefuji, M., Nakagawa, M., Izumi, N., Akiyama, T., and Kaibuchi, K. (2004). Interaction of IQGAP1 links APC to Rac1, Cdc42, and actin filaments during cell polarization and migration. Dev. Cell *7*, 871–883.

Yoshimura, T., Kawano, Y., Arimura, N., Kawabata, S., Kikuchi, A., and Kaibuchi, K. (2005). GSK-3β regulates phosphorylation of CRMP-2 and neuronal polarity. Cell *120*, 137–149.

Zhou, G., Zhuo, Y., King, C.C., Fryer, B.H., Bokoch, G.M., and Field, J. (2003). Akt phosphorylation of serine 21 on Pak1 modulates Nck binding and cell migration. Mol. Cell. Biol. *23*, 8058–8069.

Accession Numbers

The human Girdin cDNA sequence has been deposited in GenBank/EMBL/DDBJ with the accession number AB201172.

Available online at www.sciencedirect.com
SCIENCE DIRECT®
Biochemical and Biophysical Research Communications 327 (2005) 894–899
BBRC
www.elsevier.com/locate/ybbrc

Prion protein with Y145STOP mutation induces mitochondria-mediated apoptosis and PrP-containing deposits in vitro

Naomi S. Hachiya[a,b], Kota Watanabe[a,b], Makiko Y. Kawabata[a,b], Akiko Jozuka[a,b], Yoshimichi Kozuka[c], Yuji Sakasegawa[a], Kiyotoshi Kaneko[a,b,*]

[a] *Department of Cortical Function Disorders, National Institute of Neuroscience (NIN), National Center of Neurology and Psychiatry (NCNP), Kodaira, Tokyo 187-8502, Japan*
[b] *Core Research for Evolutional Science and Technology (CREST), Japan Science and Technology Corporation, Japan*
[c] *Department of Ultrastructural Research, National Institute of Neuroscience (NIN), National Center of Neurology and Psychiatry (NCNP), Kodaira, Tokyo 187-8502, Japan*

Received 2 December 2004
Available online 29 December 2004

Abstract

A pathogenic truncation of an amber mutation at codon 145 (Y145STOP) in Gerstmann–Straussler–Scheinker disease (GSS) was investigated through the real-time imaging in living cells, by utilizing GFP-PrP constructs. GFP-PrP(1–144) exhibited an aberrant localization to mitochondria in mouse neuroblastoma neuro2a (N2a) and HpL3-4 cells, a hippocampal cell line established from *prnp* gene-ablated mice, whereas full-length GFP-PrP did not. The aberrant mitochondrial localization was also confirmed by Western blot analysis. Since GFP-PrP(1–121), as previously reported, and full-length GFP-PrP do not exhibit such mitochondrial localization, the mitochondrial localization of GFP-PrP(1–144) requires not only PrP residues 121–144 (in human sequence) but also COOH-terminal truncation in the current experimental condition. Subsequently, the GFP-PrP(1–144) induced a change in the mitochondrial innermembrane potential ($\Delta\Psi_m$), release of cytochrome *c* from the intermembrane space into the cytosol, and DNA fragmentation in these cells. Non-fluorescent PrP(1–144) also induced the DNA fragmentation in N2a and HpL3-4 cells after the proteasomal inhibition. These data may provide clues as to the molecular mechanism of the neurotoxic property of Y145STOP mutation. Furthermore, immunoelectron microscopy revealed numerous electron-dense deposits in mitochondria clusters of GFP-PrP(1–144)-transfected N2a cells, whereas no deposit was detected in the cells transfected with full-length GFP-PrP. Co-localization of GFP/PrP-immunogold particles with porin-immunogold particles as a mitochondrial marker was observed in such electron-dense vesicular foci, resembling those found in autophagic vacuoles forming secondary lysosomes. Whether such electron-dense deposits may serve as a seed for the growth of amyloid plaques, a characteristic feature of GSS with Y145STOP, awaits further investigations.

Keywords: Cellular prion protein; Green fluorescent protein; PrP Y145STOP mutation; Mitochondria-mediated apoptosis; PrP-containing deposits

Prion protein (PrP) consists of two isoforms, one is a host-encoded cellular isoform (PrP^C) and the other is an abnormal protease-resistant pathogenic isoform (PrP^{Sc}), of which the latter is a causative agent of prion disease. PrP^{Sc} stimulates the conversion of PrP^C into nascent PrP^{Sc}, and the accumulation of PrP^{Sc} leads to central nervous system dysfunction and neuronal degeneration both in humans and animals [1]. The human prion diseases include kuru, Creutzfeldt–Jakob disease, Gerstmann–Straussler–Scheinker disease (GSS), and fatal familial insomnia [2,3].

* Corresponding author. Fax: +81 42 346 1748.
E-mail address: kaneko@ncnp.go.jp (K. Kaneko).

0006-291X/$ - see front matter © 2004 Elsevier Inc. All rights reserved.
doi:10.1016/j.bbrc.2004.12.079

We previously demonstrated the microtubule-associated intracellular localization of the NH_2-terminal fluorescent PrP^C fragment [4] in mouse neuroblastoma neuro2a (N2a) and HpL3-4 cells, a hippocampal cell line established from *prnp* gene-ablated mice [5], by utilizing double-labeled PrP^C. We detected NH_2-terminally fluorescent-tagged PrP^C predominantly in the intracellular compartments, COOH-terminally fluorescent-tagged PrP^C mostly at the cell surface membranes overlapping with lipid rafts, and PrP^C in full length with the merged color in Golgi compartments. Truncated PrP^C with the amino acid residues 1–121, 1–111, and 1–91 in mouse PrP exhibited a proper distribution profile. Following real-time imaging analysis with GFP-PrP^C revealed that the discrete NH_2-terminal amino acid residues are indispensable for the anterograde and the retrograde intracellular movements of GFP-PrP^C [6]. Consistent with our reports, other groups also found the GFP-tagged version of PrP^C to be properly anchored at the cell surface and its distribution pattern to be similar to that of the endogenous PrP^C, with labeling at the plasma membrane and in an intracellular perinuclear compartment [7–11].

Meanwhile, a pathogenic truncation of an amber mutation at codon 145 (Y145STOP) in the *prnp* gene, which was identified in a Japanese patient with GSS [12], came to our notice. The Y145STOP in human *prnp* gene corresponds to Y144STOP in mouse *prnp* gene which yields a product, mouse PrP(1–143) but hereafter designated PrP(1–144), and results in intracellular accumulation if proteasomal degradation is impaired [13]. Until now, its precise subcellular localization and relevance to the neurotoxic property have not been well characterized. Hence, GFP version of PrP(1–144) transgene was constructed and transfected in two independent cell lines, N2a and HpL3-4 cells.

Here we demonstrate for the first time that GFP-PrP(1–144) exhibited an aberrant mitochondrial localization accompanied by the depolarization of mitochondrial innermembrane, cytochrome *c* release in the cytosol, DNA fragmentation, and the formation of numerous PrP-containing deposits in intracellular vacuoles resembling secondary lysosomes.

Materials and methods

Construction of GFP-PrP and GFP-PrP(1–144). GFP-PrP constructs were made as previously described [4,6], and the resulted plasmid was designated pSPOX-MHM2PrP::GFP. The mutant was amplified by PCR from the pSPOX-MHM2PrP::GFP (for amino acid residues Δ144–230 in mouse PrP) [4,6], digested with *Bam*HI and *Xho*I, and replaced with the *Bam*HI–*Xho*I fragment of pSPOX-MHM2PrP::GFP [14]. Non-fluorescent PrP constructs were made from the pSPOX-MHM2PrP [14]. The resulted plasmid was verified by direct DNA sequencing.

Antibodies and drugs. Antibody K3 against PrP^C was rabbit polyclonal sera raised against N-terminal PrP peptides corresponding to residues 76–90 in mouse PrP. Anti-cytochrome *c* and anti-porin were purchased from BD Biosciences. Anti-Hsc70 and anti-BiP were purchased from Stressgen Biotechnologies. Anti-GFP was purchased from Sigma. Mitotracker Red CMXRos was purchased from Molecular Probes. Lactacystin, ALLN, and MG132 were purchased from Sigma. The mitochondrial innermembrane potential ($\Delta\Psi_m$) detection kit was purchased from Trevigen. DNA fragmentation was measured by TUNEL (APO-BrdU TUNEL assay kit (Molecular Probes)), which was performed according to the manufacturer's instructions before being visualized with a Delta-Vision microscopy system (Applied Precision), and out-of-focus images were removed by interactive deconvolution. Antibodies were used at 1:1000 (Western blotting) or 1:100 (immunoelectron microscopy) unless otherwise noted. For immunoelectron microscopy, 10 and 20 nm golds were purchased from DAKO.

Cell cultures, DNA transfection, and drug treatments. Mouse N2a cells were obtained from American Tissue Culture Collection, and HpL3-4 cells were provided by Dr. T. Onodera (the University of Tokyo). Cells were grown and maintained at 37 °C in MEM supplemented with 10% fetal bovine serum. N2a and HpL3-4 cells were transiently transfected with each construct using a DNA transfection kit (Lipofectamin, Gibco-BRL). Western blot analyses were performed as described [14]. To inhibit proteasomal function, N2a or HpL3-4 cells were treated with 10 μM lactacystin, ALLN, or MG132 for 3.5 h at 37 °C.

Preparation of mitochondrial, microsomal, and cytosolic fractions [15]. Cells were homogenized with 9 volumes of mitochondrial buffer (220 mM mannitol, 70 mM sucrose, 10 mM Hepes–KOH, pH 7.4, and 0.1 mM EDTA) and centrifuged at 700*g* for 5 min at 4 °C, and the supernatant was further centrifuged at 5000*g* for 10 min at 4 °C. The supernatant was used as a post-mitochondrial supernatant. The resulted pellet was washed three times with mitochondrial buffer, resuspended in 9 volumes of the same buffer, and then centrifuged at 2000*g* for 2 min at 4 °C followed by 5000*g* for 8 min at 4 °C. The pellet was resuspended in 9 volumes of the same buffer and then centrifuged at 5000*g* for 10 min at 4 °C. The final pellet was recovered and stored on ice until use (mitochondrial fraction). The post-mitochondrial supernatant was further centrifuged at 100,000*g* for 1 h at 4 °C, and the supernatant was used as cytosolic fraction, and the pellet was resuspended in mitochondrial buffer (microsomal fraction). Western blots were performed at 5 μg total protein/lane.

Real-time imaging. To observe living cells, cells were cultured on glass-bottomed dishes (Matsunami) for 24–48 h after the DNA transfection. To visualize mitochondria, cells were incubated for 10 min at 37 °C with Mitotracker Red CMXRos at desired concentrations. Images of cells were collected with a Delta Vision Microscopy System (Applied Precision) equipped with an Olympus IX70.

Results

The intracellular localization of fluorescent PrP^C was investigated through the real-time imaging in living cells by utilizing GFP-PrP constructs. It was investigated in N2a cells that can be infected with PrP^{Sc} [16] and has been widely used for studies in the PrP^C metabolism, as well as in HpL3-4 cells, a hippocampal cell line established from *prnp* gene-ablated mice [5].

GFP-PrP(1–144) exhibited an aberrant localization to mitochondria, as demonstrated by its colocalization with the mitochondrial-specific molecule, Mitotracker, in N2a cells (Fig. 1A, upper panels) and HpL3-4 cells (Fig. 1A, lower panels), whereas full-length GFP-PrP did not. Previously, we also demonstrated that GFP-

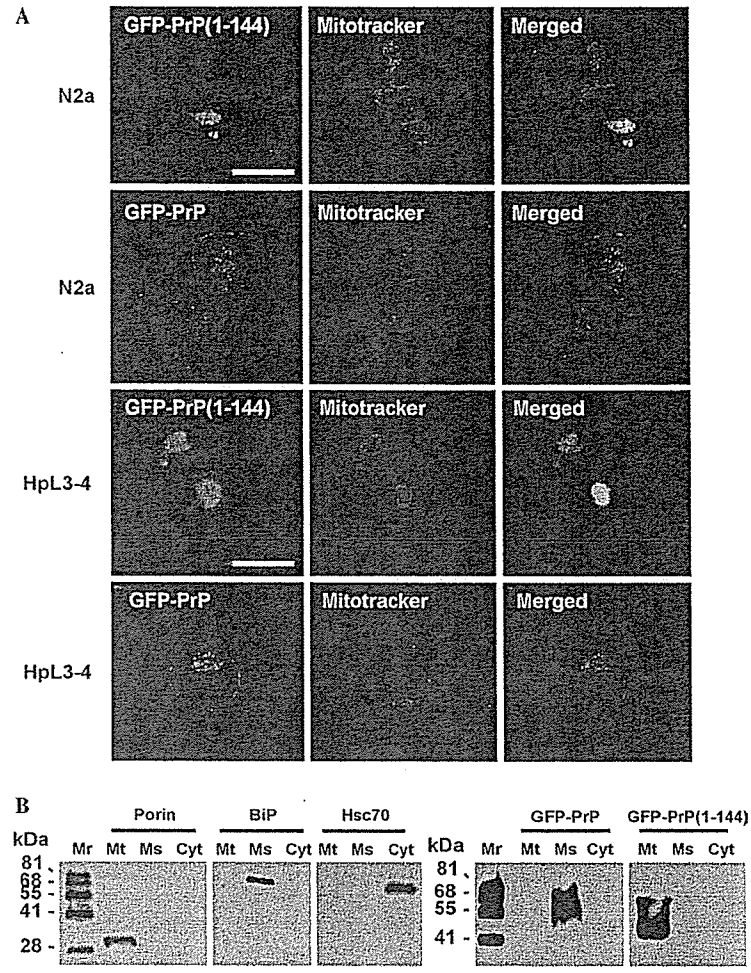

Fig. 1. Mitochondrial localization of GFP-PrP(1–144). GFP-PrP(1–144) exhibits aberrant localization in N2a cells, whereas full-length GFP-PrP does not. (A) GFP-PrP^C localization. Full-length GFP-PrP and GFP-PrP(1–144) constructs were made and transfected in N2a (upper panels) and HpL3-4 cells (lower panels). Scale bars = 8 μm. (B) Western blot analysis with anti-GFP antibody. Anti-porin antibody was used as a mitochondrial (Mt) marker, anti-BiP antibody was used as a microsome (Ms) marker, and anti-Hsc70 antibody was used as a cytosolic (Cyt) marker. Mr, molecular weight marker.

PrP(1–121) does not exhibit such mitochondrial localization [4]. Thus, the mitochondrial localization of GFP-PrP(1–144) requires not only PrP residues 121–144 (in human sequence) but also COOH-terminal truncation in the current experimental condition, regardless of whether endogenous full-length PrP^C exists. The aberrant mitochondrial localization of GFP-PrP(1–144) was further confirmed by Western blot analysis using a subcellular fractionation method (Fig. 1B).

Subsequently, the GFP-PrP(1–144) induced the depolarization of mitochondrial innermembrane (a change in the $\Delta\Psi_m$) in N2a (Fig. 2A, upper panels) and HpL3-4 cells (Fig. 2A, lower panels), release of cytochrome *c* from the intermembrane space into the cytosol (Fig. 2B), and DNA fragmentation assessed by TUNEL in N2a (Fig. 2C, upper panels) and HpL3-4 cells (data not shown). The PrP(1–144) is normally degraded through the proteasomal pathway, but intracellular accumulation results if proteasomal degradation is impaired [13]. Therefore, we next set out to treat the non-fluorescent PrP(1–144)-transfected cells with proteasome inhibitors including lactacystin, ALLN, or MG132. After the lactacystin treatment, non-fluorescent PrP(1–144) induced the DNA fragmentation in N2a (Fig. 2C, lower panels) and HpL3-4 cells (data not shown). Treatment with ALLN or MG132 also exhibited similar results (data not shown). These observations are characteristic of the mitochondria-mediated apoptotic process. In contrast, none of these abnormalities was observed in N2a and HpL3-4 cells transfected with full-length GFP-PrP construct.

During these investigations, we noticed that GFP-PrP(1–144)-transfected N2a and HpL3-4 cells lost its normal mitochondrial configurations as if congregated predominantly in an intracellular perinuclear region. To further investigate the ultrastructural

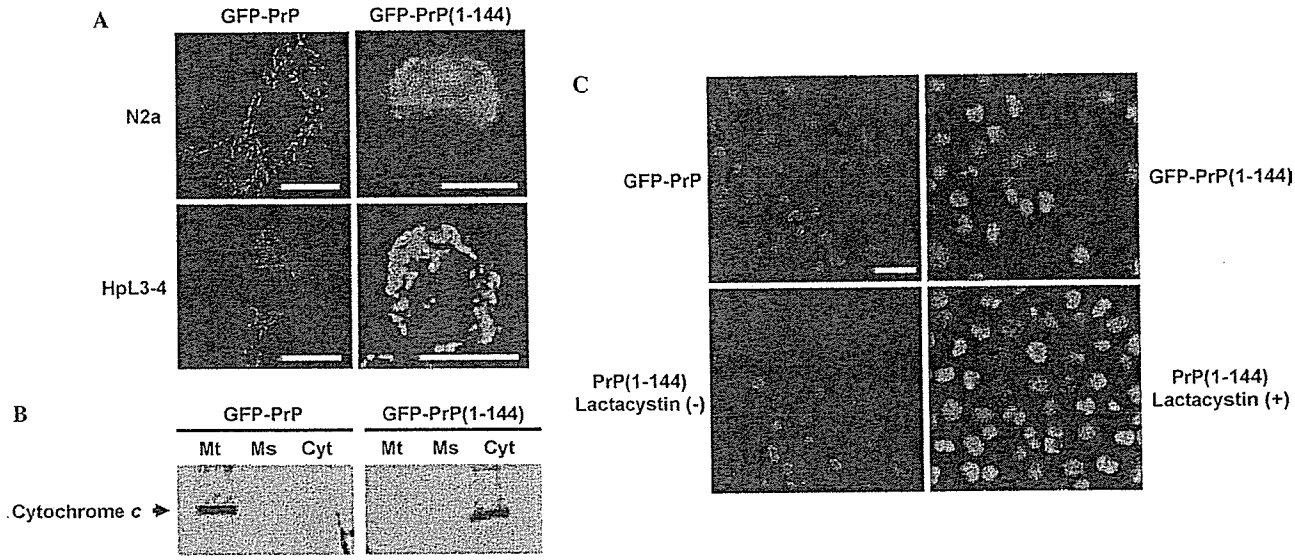

Fig. 2. Accumulation of GFP-PrP(1–144) induces mitochondria-mediated apoptosis. (A) Inactivation of the mitochondrial innermembrane potential ($\Delta\Psi_m$, red; active, green; inactive) in N2a (upper panels) and HpL3-4 (lower panels) cells transfected with GFP-PrP(1–144). Scale bars = 4 μm. (B) The release of cytochrome *c* from the mitochondria in N2a cells transfected with GFP-PrP(1–144). Mt, mitochondria fraction; Ms, microsome fraction; and Cyt, cytosolic fraction. The markers are the same as shown in Fig. 1B. (C) Upper panels: DNA fragmentations measured by TUNEL (red; negative, green; positive) are shown in N2a cells transfected with GFP-PrP(1–144). Lower panels: non-fluorescent PrP(1–144) transfected in N2a cells also exhibits the DNA fragmentation in a lactacystin-dependent manner. Scale bars = 15 μm.

morphology of these mitochondria, we next performed electron microscopy in N2a cells transfected with GFP-PrP(1–144) in comparison with full-length GFP-PrP.

As results, numerous electron-dense deposits were observed in mitochondrial clusters of the GFP-PrP(1–144)-transfected N2a cells, whereas none was detected in N2a cells transfected with full-length GFP-PrP (Fig. 3A). Some vesicles contained myelin-like figures resembling those found in autophagic vacuoles forming secondary lysosomes (Fig. 3B). Co-localization of PrP-immunogolds (Fig. 3C, left panel)/GFP-immunogolds (Fig. 3C, middle panel) with porin-immunogold particles as a mitochondrial marker (Fig. 3C, right panel) was observed in such electron-dense vesicular foci. Non-fluorescent PrP(1–144) also induced the same deposits after the proteasomal inhibition (data not shown).

Discussion

The Y145STOP mutation at PrP residue 145 results in a heritable human prion disease, GSS-like disorder, with extensive PrP amyloid deposits in cerebral parenchyma and vessels [12,17]. The Y145STOP, which yields a product of PrP(1–144), lacks GPI-anchor and is normally degraded through the proteasomal pathway, and also results in intracellular accumulation if proteasomal degradation is impaired [13]. Most PrP(1–144) is degraded very rapidly by the proteasome-mediated pathway, and thus blockage of proteasomal degradation results in intracellular accumulation of PrP(1–144). From the current results, however, the GFP-tagged PrP(1–144) seems to be more metabolically stable, and therefore GFP-PrP(1–144) expression itself is sufficient to induce its intracellular accumulation. In fact, non-fluorescent PrP(1–144) required the treatment with proteasome inhibitors to exhibit the same features.

In this paper, we revealed for the first time the site of intracellular accumulation and the neurotoxic property of mutant PrP^C, Y145STOP, in a human GSS model. The GFP-PrP(1–144) exhibited an aberrant localization to mitochondria, and subsequent mitochondria-mediated apoptosis was induced. Misfolded PrP^C is subjected to degradation by proteasomes, and accumulation of PrP^C in the cytosol is strongly neurotoxic in transgenic mice [18] and cyclosporin A-treated cultured cells [19], and proteasome inhibitors increase PrP^C-like immunoreactivity and unmasked a basal caspase 3 activation [20]. Concomitant with decreased proteasomal activity, aberrant mitochondrial localization of PrP^C followed by mitochondria-mediated neuronal apoptosis was also detected in aged transgenic mice overexpressing wild-type mouse PrP^C, but only after 520 days after birth [15]. These mice develop a spontaneous neurological dysfunction in an age-dependent manner [21,22]. Taken together, a PrP^C load in the cytosol induces the mitochondrial localization of PrP^C with subsequent mito-

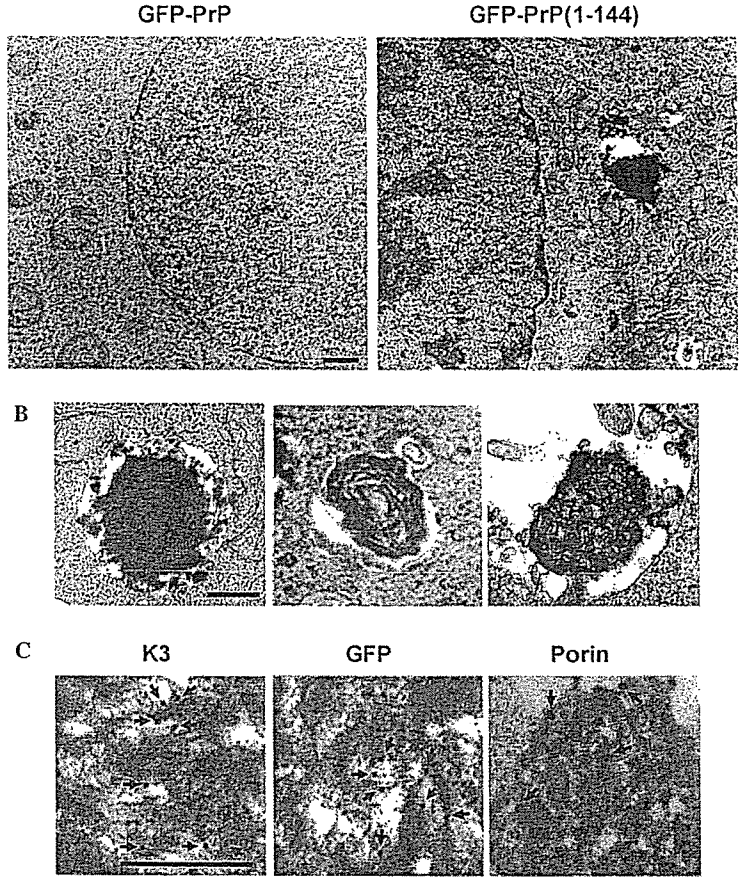

Fig. 3. GFP-PrP(1–144)-related electron-dense deposits. Scale bars = 0.1 μm. (A) Electron microscopy (30,000×) detects numerous electron-dense deposits in N2a cells transfected with GFP-PrP(1–144), whereas full-length GFP-PrP induces no deposit. (B) Some vesicles contain myelin-like figures. (C) Immunoelectron microscopy (30,000×) detects GFP-PrP(1–144) with anti-PrP antibody K3 (10 nm golds, left panel) or anti-GFP antibody (10 nm golds, middle panel) within the electron dense deposits of N2a cells. Anti-porin antibody (20 nm golds) also stains the deposits (right panel).

chondria-mediated apoptosis. Consequently, such neurotoxic property may contribute to a common pathogenic mechanism shared in various PrP-related disorders.

Deposition of numerous electron-dense deposits immunostained with anti-PrP antibody is another characteristic in GFP-PrP(1–144)-transfected cells, and has not been reported in other studies so far. The relevance of such electron-dense deposits with PrP amyloid deposits, a characteristic feature of human GSS with Y145STOP, is an intriguing question. These amyloid plaques were composed of COOH-terminal truncated PrP [12], but have not transmitted to mice [17]. Of note, both the electron-dense deposits in Y145STOP-transfected N2a cells and PrP^{Sc} in scrapie-infected N2a cells were found in the similar vacuolar compartment resembling secondary lysosomes [23], suggesting that both deposits may share a similar resistance to such a harsh lysosomal condition.

The Y145STOP mutation has been widely investigated in terms of its biochemical property. Peptides encompassing PrP(89–143) when mixed with PrP^{C} produced fibrous aggregates and displayed a high β-sheet content, although no prion infectivity was observed [24,25]. Recently, Kundu et al. [26] reported a spontaneous conversion of the recombinant polypeptide, human PrP(23–144), from a monomeric unordered state to a fibrillar form, in which human PrP residues within the 138–141 region are essential. Interestingly, this conversion has characteristics of a nucleation-dependent polymerization. Whether the numerous electron-dense deposits may serve as a seed for the growth of amyloid plaques with Y145STOP awaits further investigations.

Our current observations may provide clues as to the yet unknown underlying mechanism concerning the heritable human prion disease with Y145STOP at least in part. At the same time, the prion disease with Y145STOP has untransmitted to mice [17]. How this relates to the puzzle in prion biology, the discrepancy between the infectious and neurotoxic properties of PrP [27], remains to be further examined.

Acknowledgments

We greatly thank T. Onodera for providing the HpL3-4 cell line, E. Nannri, K. Ishibashi, C. Ota, and S. Wajima for technical assistances. This work was supported by grants from the Core Research for Evolutional Science and Technology (CREST) of Japan Science and Technology Corporation, Health and Labour Sciences Research Grants, Research on Advanced Medical Technology, nano-001, the Ministry of Agriculture, Forestry and Fisheries, and the Ministry of Health, Labor, and Welfare of Japan.

References

[1] S.B. Prusiner, Prions, Proc. Natl. Acad. Sci. USA 95 (1998) 13363–13383.
[2] S.B. Prusiner, Shattuck lecture—neurodegenerative diseases and prions, N. Engl. J. Med. 344 (2001) 1516–1526.
[3] J. Collinge, Variant creutzfeldt-Jakob disease, Lancet 354 (1999) 317–323.
[4] N.S. Hachiya, K. Watanabe, Y. Sakasegawa, K. Kaneko, Microtubules-associated intracellular localization of the NH(2)-terminal cellular prion protein fragment, Biochem. Biophys. Res. Commun. 313 (2004) 818–823.
[5] C. Kuwahara, A.M. Takeuchi, T. Nishimura, K. Haraguchi, A. Kubosaki, Y. Matsumoto, K. Saeki, T. Yokoyama, S. Itohara, T. Onodera, Prions prevent neuronal cell-line death, Nature 400 (1999) 225–226.
[6] N.S. Hachiya, K. Watanabe, M. Yamada, Y. Sakasegawa, K. Kaneko, Anterograde and retrograde intracellular trafficking of fluorescent cellular prion protein, Biochem. Biophys. Res. Commun. 315 (2004) 802–807.
[7] K.S. Lee, A.C. Magalhaes, S.M. Zanata, R.R. Brentani, V.R. Martins, M.A. Prado, Internalization of mammalian fluorescent cellular prion protein and N-terminal deletion mutants in living cells, J. Neurochem. 79 (2001) 79–87.
[8] A.C. Magalhaes, J.A. Silva, K.S. Lee, V.R. Martins, V.F. Prado, S.S.G. Ferguson, M.V. Gomez, R.R. Brentani, M.A.M. Prado, Endocytic intermediates involved with the intracellular trafficking of a fluorescent cellular prion protein, J. Biol. Chem. 277 (2002) 33311–33318.
[9] A. Negro, C. Ballarin, A. Bertoli, M.L. Massimino, M.C. Sorgato, The metabolism and imaging in live cells of the bovine prion protein in its native form or carrying single amino acid substitutions, Mol. Cell. Neurosci. 17 (2001) 521–538.
[10] H. Lorenz, O. Windl, H.A. Kretzschmar, Cellular phenotyping of secretory and nuclear prion proteins associated with inherited prion diseases, J. Biol. Chem. 277 (2002) 8508–8516.
[11] L. Ivanova, S. Barmada, T. Kummer, D.A. Harris, Mutant prion proteins are partially retained in the endoplasmic reticulum, J. Biol. Chem. 276 (2001) 42409–42421.
[12] T. Kitamoto, R. Iizuka, J. Tateishi, An amber mutation of prion protein in Gerstmann–Straussler syndrome with mutant PrP plaques, Biochem. Biophys. Res. Commun. 192 (1993) 525–531.
[13] G. Zanusso, R.B. Petersen, T. Jin, Y. Jing, R. Kanoush, S. Ferrari, P. Gambetti, N. Singh, Proteasomal degradation and N-terminal protease resistance of the codon 145 mutant prion protein, J. Biol. Chem. 274 (1999) 23396–23404.
[14] M.R. Scott, R. Kohler, D. Foster, S.B. Prusiner, Chimeric prion protein expression in cultured cells and transgenic mice, Protein Sci. 1 (1992) 986–997.
[15] N.S. Hachiya, M. Yamada, K. Watanabe, A. Jozuka, T. Ohkubo, K. Sano, Y. Takeuchi, Y. Kozuka, Y. Sakasegawa, K. Kaneko, Mitochondrial localization of cellular prion protein (PrPC) invokes neuronal apoptosis in aged transgenic mice overexpressing PrPC, Neurosci. Lett., in press.
[16] D.A. Butler, M.A. Scott, J.M. Bockman, D.R. Borchelt, A. Taraboulos, K.K. Hsiao, D.T. Kingsbury, S.B. Prusiner, Scrapie-infected murine neuroblastoma cells produce protease-resistant prion proteins, J. Virol. 62 (1988) 1558–1564.
[17] J. Tateishi, T. Kitamoto, Inherited prion diseases and transmission to rodents, Brain Pathol. 5 (1995) 53–59.
[18] J. Ma, R. Wollmann, S. Lindquist, Neurotoxicity and neurodegeneration when PrP accumulates in the cytosol, Science 298 (2002) 1781–1785.
[19] E. Cohen, A. Taraboulos, Scrapie-like prion protein accumulates in aggresomes of cyclosporin A-treated cells, EMBO J. 22 (2003) 404–417.
[20] E. Paitel, C. Alves da Costa, D. Vilette, J. Grassi, F. Checler, Overexpression of PrPc triggers caspase 3 activation: potentiation by proteasome inhibitors and blockade by anti-PrP antibodies, J. Neurochem. 83 (2002) 1208–1214.
[21] D. Westaway, J. Cayetano-Canlas, D. Groth, D. Foster, S.-L. Yang, M. Torchia, G.A. Carlson, S.B. Prusiner, Degeneration of skeletal muscle, peripheral nerves, and the central nervous system in transgenic mice overexpressing wild-type prion proteins, Cell 76 (1994) 117–129.
[22] V. Perrier, K. Kaneko, J. Safar, J. Vergara, P. Tremblay, S.J. DeArmond, F.E. Cohen, S.B. Prusiner, A.C. Wallace, Dominant-negative inhibition of prion replication in transgenic mice, Proc. Natl. Acad. Sci. USA 99 (2002) 13079–13084.
[23] M.P. McKinley, A. Taraboulos, L. Kenaga, D. Serban, A. Stieber, S.J. DeArmond, S.B. Prusiner, N. Gonatas, Ultrastructural localization of scrapie prion proteins in cytoplasmic vesicles of infected cultured cells, Lab. Invest. 65 (1991) 622–630.
[24] K. Kaneko, D. Peretz, K.M. Pan, T.C. Blochberger, H. Wille, R. Gabizon, O.H. Griffith, F.E. Cohen, M.A. Baldwin, S.B. Prusiner, Prion protein (PrP) synthetic peptides induce cellular PrP to acquire properties of the scrapie isoform, Proc. Natl. Acad. Sci. USA 92 (1995) 11160–11164.
[25] K. Kaneko, H. Wille, I. Mehlhorn, H. Zhang, H. Ball, F.E. Cohen, M.A. Baldwin, S.B. Prusiner, Molecular properties of complexes formed between the prion protein and synthetic peptides, J. Mol. Biol. 270 (1997) 574–586.
[26] B. Kundu, N.R. Maiti, E.M. Jones, K.A. Surewicz, D.L. Vanik, W.K. Surewicz, Nucleation-dependent conformational conversion of the Y145Stop variant of human prion protein: structural clues for prion propagation, Proc. Natl. Acad. Sci. USA 100 (2003) 12069–12074.
[27] R. Chiesa, P. Piccardo, E. Quaglio, B. Drisaldi, S.L. Si-Hoe, M. Takao, B. Ghetti, D.A. Harris, Molecular distinction between pathogenic and infectious properties of the prion protein, J. Virol. 77 (2003) 7611–7622.

Available online at www.sciencedirect.com
SCIENCE DIRECT®
Neuroscience Letters 374 (2005) 98–103
Neuroscience Letters
www.elsevier.com/locate/neulet

Mitochondrial localization of cellular prion protein (PrP^C) invokes neuronal apoptosis in aged transgenic mice overexpressing PrP^C

Naomi S. Hachiya[a,b], Makiko Yamada[a,b], Kota Watanabe[a,b], Akiko Jozuka[a,b], Takuya Ohkubo[a,c], Kenichi Sano[a,1], Yoshio Takeuchi[a,2], Yoshimichi Kozuka[d], Yuji Sakasegawa[a], Kiyotoshi Kaneko[a,b,*]

[a] *Departments of a Cortical Function Disorders, National Institute of Neuroscience (NIN), National Center of Neurology and Psychiatry (NCNP), Kodaira, Tokyo 187-8502, Japan*
[b] *Core Research for Evolutional Science and Technology (CREST), Japan Science and Technology Agency, Kawaguchi, Saitama 332-0012, Japan*
[c] *Department of Neurology and Neurological Science, Graduate School of Medicine, Tokyo Medical and Dental University, Bunkyo-ku, Tokyo 113-0034, Japan*
[d] *Ultrastructural Research, National Institute of Neuroscience (NIN), National Center of Neurology and Psychiatry (NCNP), Kodaira, Tokyo 187-8502, Japan*

Received 14 September 2004; received in revised form 12 October 2004; accepted 13 October 2004

Abstract

Recent studies suggest that the disease isoform of prion protein (PrP^{Sc}) is non-neurotoxic in the absence of cellular isoform of prion protein (PrP^C), indicating that PrP^C may participate directly in the neurodegenerative damage by itself. Meanwhile, transgenic mice harboring a high-copy-number of wild-type mouse (Mo) PrP^C develop a spontaneous neurological dysfunction in an age-dependent manner, even without inoculation of PrP^{Sc} and thus, investigations of these aged transgenic mice may lead to the understanding how PrP^C participate in the neurotoxic property of PrP. Here we demonstrate mitochondria-mediated neuronal apoptosis in aged transgenic mice overexpressing wild-type $MoPrP^C$ (Tg(MoPrP)4053/FVB). The aged mice exhibited an aberrant mitochondrial localization of PrP^C concomitant with decreased proteasomal activity, while younger littermates did not. Such aberrant mitochondrial localization was accompanied by decreased mitochondrial manganese superoxide dismutase (Mn-SOD) activity, cytochrome *c* release into the cytosol, caspase-3 activation, and DNA fragmentation, most predominantly in hippocampal neuronal cells. Following cell culture studies confirmed that decrease in the proteasomal activity is fundamental for the PrP^C-related, mitochondria-mediated apoptosis. Hence, the neurotoxic property of PrP^C could be explained by the mitochondria-mediated neuronal apoptosis, at least in part.

Keywords: PrP^C; Proteasomal activity; Mitochondrial localization; Superoxide dismutase activity; Mitochondria-mediated apoptosis

The posttranslational conformational change of the cellular isoform of prion protein (PrP^C) into its scrapie isoform (PrP^{Sc}) is the fundamental process underlying the pathogenesis of prion diseases [24], but the molecular events through which prion infection and the resulting accumulation of PrP lead to the neuronal dysfunction, vacuolation, and death that characterize prion pathology remain unclear [6].

Importantly, PrP^{Sc}, the disease isoform of PrP, seems to be non-neurotoxic in the absence of PrP^C, suggesting that PrP^C may participate directly in the prion neurodegenerative damage by itself, and the cellular pathways activated by neurotoxic forms of PrP that ultimately result in neuronal death are also being investigated, and several possible mechanisms have been uncovered [6]. For example, cross-linking

* Corresponding author. Tel.: +81 42 346 1718; fax: +81 42 346 1748.
E-mail address: kaneko@ncnp.go.jp (K. Kaneko).
[1] Present address: Hinoieda Kagaku Ltd., Hino-city, Tokyo 191-0061, Japan.
[2] Present address: KOHJIN-BIO Ltd., Sakado-city, Saitama 350-0214, Japan.

0304-3940/$ – see front matter © 2004 Elsevier Ireland Ltd. All rights reserved.
doi:10.1016/j.neulet.2004.10.044

PrP^C in vivo with specific monoclonal antibodies was found to trigger neuronal apoptosis, suggesting that PrP^C functions in the control of neuronal survival [26]. In fact, neural tissues overexpressing PrP^C grafted into the brains of PrP^C-deficient mice develop the severe histopathological changes characteristic of prion disease when infected with prions, but no pathological changes were seen in PrP^C-deficient tissue, not even in the immediate vicinity of the grafts despite the presence of high levels of PrP^{Sc} [2]. In addition, interruption of PrP^C expression during an ongoing prion infection prevents neuronal loss and reverses early spongiform change [16]. The continued accumulation of PrP^{Sc} in this model after neuronal PrP^C depletion is likely to reflect prion replication predominantly in both microglia and astrocytes glial cells without PrP^C depletion, which support PrP^{Sc} replication. The PrP^{Sc} deposits colocalize with astrocytes in the brains of infected mice with neuronal PrP^C depletion, which was not seen in scrapie-infected control animals without PrP depletion. The fact that these mice remain asymptomatic indicates that even extensive extraneuronal PrP^{Sc} replication does not cause clinical disease or neurodegeneration in this model. Thus, neuronal PrP^C seems to be fundamental for the neurotoxic property of PrP even in the PrP^{Sc}-infected conditions, but the detailed molecular events especially with non-mutant, wild-type PrP^C still remained unclear.

Meanwhile, aged transgenic mice harboring a high-copy-number of wild-type PrP-B transgenes spontaneously developed mitochondrial encephalomyopathy including focal vacuolation of the central nervous system, skeletal muscles and peripheral nerves without PrP^{Sc} inoculation [28]. Such focal vacuolation was localized to the hippocampus, the superior colliculus, and midbrain tegmentum, which resembled that seen in experimental scrapie, albeit less intense. Other transgenic lines harboring a high-copy-number of wild-type PrP transgenes also exhibited spontaneous neurological dysfunction in an age-dependent manner [21,27]. For example, transgenic mice overexpressing the wild-type mouse (Mo) PrP-A gene (Tg(MoPrP)4053/FVB) used in this study became symptomatic at around the age of 700 days, although no pathological evidence for prion diseases was evident [27]. Since no PrP^{Sc} has been inoculated in these mice, investigations of these aged transgenic mice overexpressing wild-type PrP^C may lead to the better understanding how PrP^C participate in the neurotoxic property of PrP.

Here we show that the Tg(MoPrP)4053/FVB mice exhibited an aberrant mitochondrial localization of PrP^C accompanied by decreased mitochondrial manganese superoxide dismutase (Mn-SOD) activity, cytochrome *c* release in the cytosol, caspase-3 activation, and DNA fragmentation, concomitant with decreased proteasomal activity in an age-dependent manner.

Tg(MoPrP)4053/FVB and its littermate were kindly provided by Dr. S.B. Prusiner (University of California, San Francisco). Antibodies K3 and K4 against PrP were rabbit polyclonal sera raised against PrP peptides corresponding to residues 76–90 and 96–110 in MoPrP, respectively. Anti-cytochrome *c* and anti-porin antibodies were purchased from BD Biosciences. Anti-Hsc70 antibody was purchased from Stressgen Biotechnologies Corporation. Mitotracker Red CMXRos was purchased from Molecular Probes. Lactacystin, ALLN, and MG132 were purchased from Sigma. The $\Delta\Psi m$ detection kit and APO-BrdU TUNEL assay kit were purchased from Trevigen Inc. and Molecular Probes, respectively. Antibodies were used at 1:1000 (Western blotting) or 1:100 (immunofluorescence microscopy) unless otherwise noted. For immuno-electronmicroscopy, 10 nm golds were purchased from DAKO.

Cells or brains were homogenized with 9 volumes of mitochondrial buffer (220 mM mannitol, 70 mM sucrose, 10 mM Hepes-KOH, pH 7.4, and 0.1 mM EDTA) and centrifuged at $700 \times g$ for 5 min at 4 °C, and the supernatant was further centrifuged at $5000 \times g$ for 10 min at 4 °C. The supernatant was used as a post-mitochondrial supernatant. The resulted pellet was washed three times with mitochondrial buffer, resuspended in 9 volumes of the same buffer, and then centrifuged at $2000 \times g$ for 2 min at 4 °C followed by $5000 \times g$ for 8 min at 4 °C. The pellet was resuspended in 9 volumes of the same buffer, and then centrifuged at $5000 \times g$ for 10 min at 4 °C. The final pellet was recovered and stored on ice until use (mitochondrial fraction). The post-mitochondrial supernatant was further centrifuged at $100{,}000 \times g$ for 1 h at 4 °C, and the supernatant was used as cytosolic fraction, and the pellet was resuspended in mitochondrial buffer (microsome fraction). Western blots were performed at 5 μg of total protein/lane.

Mitochondrial manganese superoxide dismutase (Mn-SOD) and cytosolic copper/zinc SOD (Cu/Zinc-SOD) activities were measured by the SOD assay kit (Dojindo Molecular Technologies, Inc.), and cytosolic glutathione (GSH) was measured by the Glutathione quantification kit (Dojindo Molecular Technologies, Inc.) according to the manufacturer's instructions. Caspase-3 activity was measured using the PARP Western Blot Kit (WAKO) according to the manufacturer's instructions. DNA fragmentation was measured by the TUNEL assay (ApopTag® Peroxidase *In situ* Apoptosis Detection Kit, CHEMICON International), which was performed according to the manufacturer's instructions before being visualized with an Olympus CX40 (Olympus Optical Co., Ltd.). Sections were counter-stained by 0.5% methyl green (WAKO) in 0.1 M sodium acetate (pH 4.0).

Proteasomal activity assay was performed as previously described [3,9,31].

Tg(MoPrP)4053/FVB harboring a high-copy-number of wild-type PrP-A transgenes at the age of 520 days (TG520) and an age-matched non-transgenic littermate (WT520) showed similar migration rates of PrP^C on poly acrylamide gel electrophoresis and Western blotting using anti-PrP-antibody K4 (Fig. 1A, PK(−)). As increased resistance to protease K digestion is often a feature of PrP^{Sc}, this was examined in TG520 and WT520. No resistance to proteinase K digestion was detected in any of these mice (Fig. 1A, PK(+)). Histological examinations of the TG520 brains including

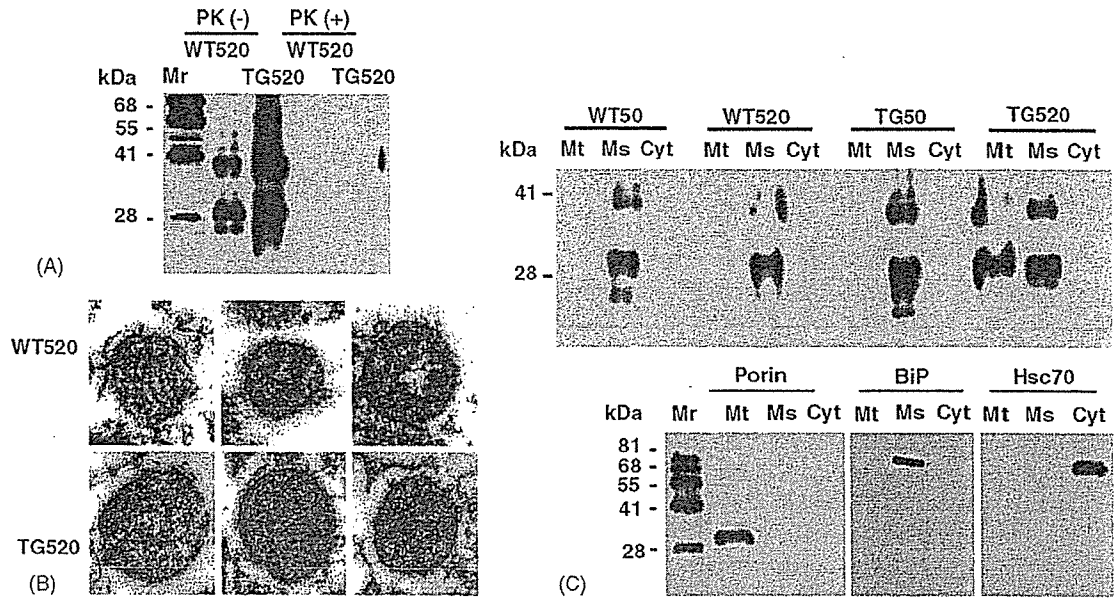

Fig. 1. PrP^C is localized to the mitochondrial fraction in Tg(MoPrP)4053/FVB overexpressing wild-type PrP^C. WT520: non-transgenic littermate at the age of 520 days. TG520: Tg(MoPrP)4053/FVB at the age of 520 days. WT50: non-transgenic littermate at the age of 50 days. TG50: Tg(MoPrP)4053/FVB at the age of 50 days. (A) Western blot analysis and resistance to proteinase K digestion of PrP^C in WT520 and TG520. PK(−): Western blot analysis with anti-PrP antibody K4. Bands derived from PrP^C appear to be normal. PK(+): resistance to proteinase K digestion. Five hundred microliter of brain homogenates (5 μg of total protein/lane) were digested with proteinase K (20 μg/ml, Sigma) at 37 °C for 1 h followed by centrifugation at 100,000 × *g* for 1 h at 4 °C and the resuspended pellet was loaded onto the gels. No resistance to proteinase K digestion is detected. Mr: molecular weight marker. (B) Immuno electron microscopy (30,000×) detects PrP^C with anti-PrP K3 (10 nm golds) in the mitochondria of neuronal cells in TG520. (C) Total brain homogenates of TG520 exhibit aberrant localization of overexpressed PrP^C, whereas those of WT50, WT520 and TG50 do not. Western blot analysis with anti-PrP antibody K4 (1:1000). Anti-porin antibody (1:1000) was used as a mitochondrial (Mt) marker, anti-BiP antibody (1:1000) was used as a microsome (Ms) marker, and anti-Hsc70 antibody (1:1000) was used as a cytosolic (Cyt) marker.

dentate gyrus, hippocampus, other cerebral cortices, basal ganglia and cerebellum by hematoxylin and eosin as well as methyl green-pyronin staining revealed no apparent pathological evidence in the brain sections of WT520 and TG520 (data not shown).

Since older transgenic mice (not inoculated with PrP^{Sc}) that harbor a high-copy-number of wild-type PrP-B transgenes develop mitochondrial encephalomyopathy including focal vacuolation of the central nervous system, skeletal muscles and peripheral nerves [28], we set out to determine whether PrP^C could be detected in the mitochondrial fraction of TG520. Although the TG520 appeared clinically and histologically normal, they exhibited aberrant mitochondrial localization of PrP^C as determined by immuno electron microscopy; immunogold-labelled PrP^C localized at the mitochondria of the granular cells in the hippocampal dentate gyrus of TG520 but not of WT520 (Fig. 1B). Such aberrant mitochondrial localization of PrP^C was further confirmed in TG520 by Western blotting using a subcellular fractionation, whereas younger non-transgenic littermate at the age of 50 days (WT50), WT520, and younger Tg(MoPrP)4053/FVB at the age of 50 days (TG50) did not exhibit the feature (Fig. 1C).

The oxidative stress leads to dysfunctions of the respiratory enzymes and the depletion of ATP followed by a decrease in reduced glutathione (GSH) concentration, which triggers the cycle of oxidative stress, mitochondrial dysfunction, and further antioxidant depletion. Exposure of tissue to oxygen free radicals results in lipid peroxidation, protein oxidation and DNA damage, which is in concert with "apoptosis". In order to prevent such damages, mammalian cells are equipped with both non-enzymatic and enzymatic scavenging systems to eliminate oxygen free radicals, anti oxidant enzymes, i.e., SOD, catalase, and glutathione peroxidase are essential to cells in removing O_2^- and hydrogen peroxide (H_2O_2) from the tissues exposed to oxidative stress. Therefore, we next examined mitochondrial Mn-SOD as well as cytosolic Cu/Zn-SOD activities.

The mitochondrial Mn-SOD activity decreased significantly in TG520 compared to that in WT50, TG50, or WT520 (Fig. 2A), whereas no significant difference in the cytosolic copper/zinc SOD (Cu/Zn-SOD) activity was observed among them (Fig. 2B). Furthermore, cytosolic GSH level was dramatically decreased in TG520 but not in WT50, TG50, or WT520 (Fig. 2C). These results indicated that mitochondria-localized PrP^C induced oxidative stress in TG520.

Subsequently, release of cytochrome *c* from the inner-membrane space into the cytosol (Fig. 3A), caspase-3 activation (Fig. 3B), and DNA fragmentation (Fig. 3C) were observed in TG520 brain, whereas no release of cytochrome *c*/ DNA fragmentation but faint caspase-3 activation was detected in WT520 brain (Fig. 3A–C). Serial specimens of TG520 and WT520 brains were further examined by

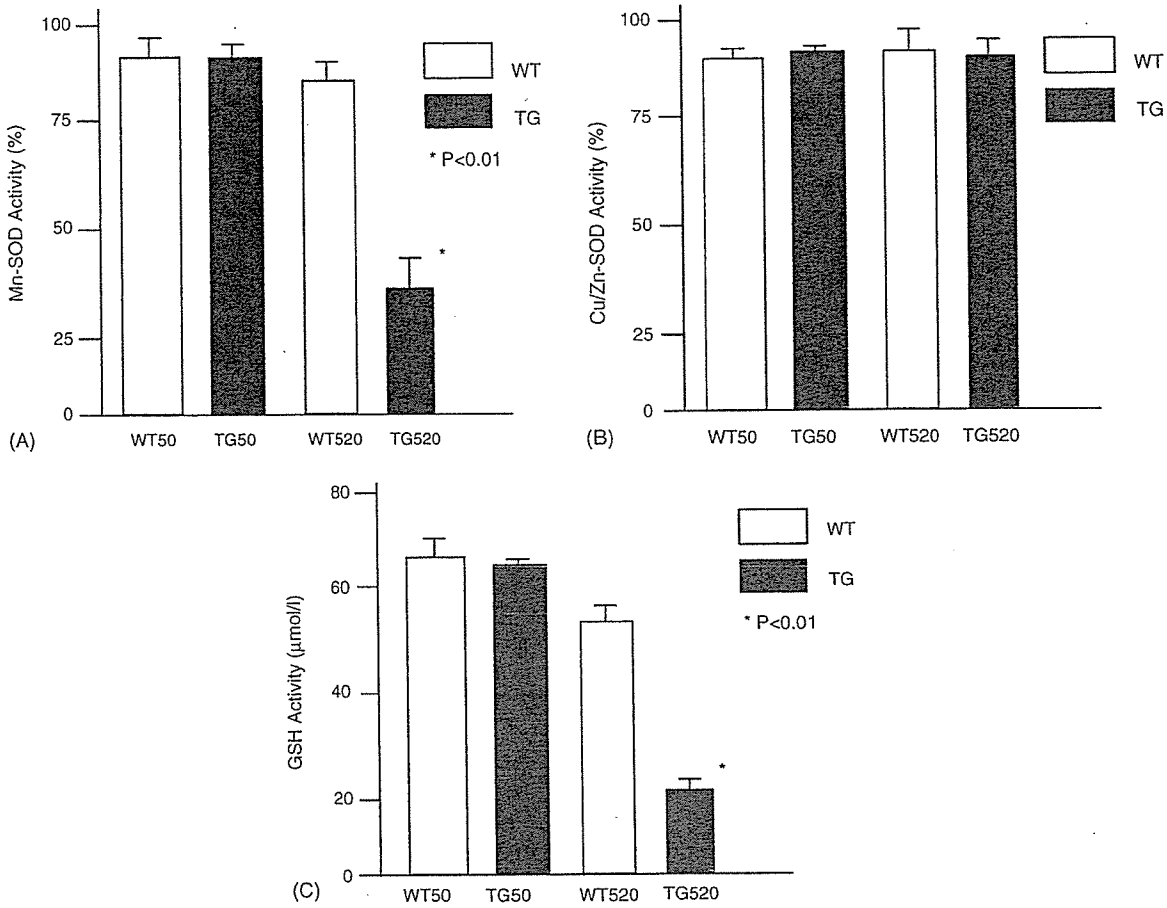

Fig. 2. Mitochondria-localized PrP^C induces oxidative stress in TG520. (A) Mitochondrial manganese superoxide dismutase (Mn-SOD) and (B) cytosolic copper/zinc SOD (Cu/Zinc-SOD) activities. The Mn-SOD activity decreases significantly in TG520 compared to that in WT50, TG50 or WT520, whereas the cytosolic Cu/Zn-SOD activity remained similar among them. Error bars represent mean ± S.D. (C) Cytosolic glutathione (GSH) level is dramatically decreased in TG520 but not in WT50, TG50, or WT520. Error bars represent mean ± S.D.

the TUNEL assay (Fig. 3D). As shown, the TUNEL assay showed that the DNA fragmentation most predominantly in granular cells in the hippocampal dentate gyrus and to a lesser extent pyramidal cells in the CA1 and CA2 regions of TG520 (Fig. 3D).

In an age-dependent development of other aggregation disorders, the accumulation and aggregation of the disease related-proteins are associated with an age-dependent decrease in proteasomal activity and are promoted by inhibition of proteasomal activity [31]. Therefore, it is also likely that such aberrant mitochondrial localization requires PrP^C retained in the cytoplasm with the proteasomal activity decreased. Therefore, the hydrolysis of Suc-Leu-Leu-Val-Tyr-4-methyl-coumaryl-7-amide (Suc-LLVY-MCA) by chymotrypsin-like proteasomal activity in brain homogenates of WT50, WT520, TG50, and TG520 was then investigated. As expected, proteasomal activity of both transgenic mice Tg(MoPrP)4053/FVB and non-transgenic littermate decreased with increasing age (Fig. 3E).

The posttranslational conformational change of PrP^C into PrP^{Sc} is the fundamental process underlying the pathogenesis of prion diseases [24]. Many concurrent reports have suggested that PrP^C may play a role in neuronal survival or death. The removal of serum from cells in culture causes apoptosis in PrP^C-deleted cells but not in wild-type cells [13]. PrP^C also inhibits Bax-mediated neuronal apoptosis in human primary neurons [1]. The binding of a ligand to PrP^C transduces neuroprotective signaling through a cAMP/PKA-dependent pathway. Therefore, PrP^C may function as a trophic receptor whose activation results in a neuroprotective state [5].

On the other hand, misfolded PrP^C is subject to degradation by proteasomes. Like many misfolded secretory proteins [12,23], it is recognized in the ER and subject to retrograde transport to the cytoplasm and degradation by the proteasome [11,14,29,30]. Or, a small fraction of PrP chains is not translocated into the ER lumen during synthesis, and is rapidly degraded in the cytoplasm by the proteasome as far as proteasome function remains normal [8]. As proteasome function gradually decreases with age over a very long period or with inhibitors in the case of cultured cells, PrP^C overflows in the cytoplasm, targeted to the mitochondria, which subsequently induces the mitochondria-mediated apoptosis.

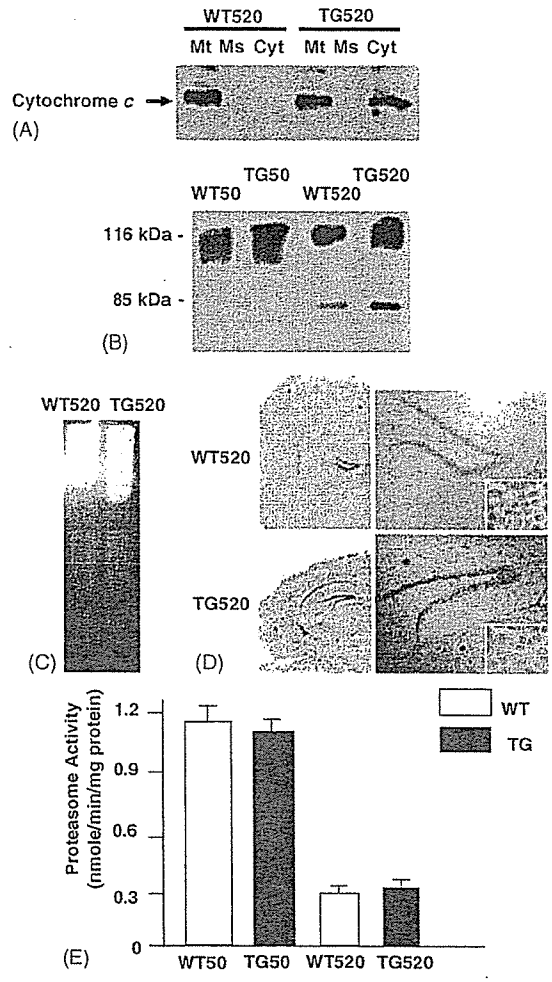

Fig. 3. Neuronal apoptosis in the TG520 brain. (A) Measurement of cytochrome *c* released into the cytosol. Western blot analysis with anti-cytochrome *c* antibody detects cytochrome *c* in the cytosol of the TG520 but not WT520 brain. Mt: mitochondrial fraction, Ms: microsome fraction, Cyt: cytosolic fraction. (B) Caspase-3 activation in TG520 brain. Brain homogenates (5 μg of total protein/lane) of younger WT50 and TG50 do not exhibit caspase-3 activation. Note that a faint band is detected in WT520 brain. The 85 kDa bands corresponding to the degradation products of poly ADP-ribose polymerase (PARP, 116 kDa) is a measure of caspase-3 activity. (C) DNA fragmentation in brain homogenates of TG520 is shown (1 μg of genomic DNA/lane). Brain homogenates of WT520 show no DNA fragmentation. Genomic DNAs were applied onto 1% agarose gel. (D) Serial frozen sections of total brains (left panels) and the hippocampal regions (right panels, 40×, lower right corner panels, 400×) were made. Top panels: WT520. Bottom panels: TG520. Neuronal apoptosis (brown) is evident in the bottom panels as compared with the top panels. (E) Age-dependent decrease in brain proteasomal activity. Chymotrypsin-like proteolytic activity was assayed in brain homogenates (1 μg of total protein/assay) of WT50, TG50, WT520, and TG520. Error bars represent mean ± S.D. ($n = 3$).

In fact, accumulation of PrP^C in the cytoplasm is known to be strongly neurotoxic in both transgenic mice overexpressing the cytosolic form of PrP^C [15] and cyclosporin A-treated cultured cells [7]. In these systems, PrP^C expression enhances staurosporine-stimulated neuronal toxicity and DNA fragmentation, caspase-3-like activity and p53 transcriptional activities, all of which suggests that PrP^C sensitizes neurons to apoptotic stimuli through caspase-3-mediated activation [20]. Proteasome inhibitors increase PrP^C-like immunoreactivity and unmask basal caspase-3 activation [19].

Despite these efforts, little is known about the PrP^C localization and its metabolic fate in the cytoplasm. Ma et al. reported that PrP accumulated in the cytoplasm when proteasomal activity was compromised, and PrP^C formed aggregates, often in association with Hsc70 [14]. With prolonged incubation, these aggregates accumulate in an "aggresome"-like state, surrounding the centrosome. Contrary to this report, other investigators reported there was a prominent shift in the intracellular locations of PrP immunostaining, but there was no "aggresome"-like PrP accumulation in the centrosome region [29]. The PrP signal was especially pronounced around the nucleus, and this signal only partially overlapped with both ER (calnexin, BiP and concanavalin A) and Golgi (wheat germ agglutinin). Thus, further examination has been awaited for determining the precise intracellular localization of PrP^C in the cytoplasmic face.

With an artificial PrP peptide corresponding to PrP residues 106–126 [PrP(106–126)], chronic exposure of primary rat hippocampal cultures to micromolar concentrations of the peptide induces neuronal death with DNA fragmentation in degenerating neurons, having indicated apoptotic cell death [10]. The earliest detectable apoptotic event was the rapid depolarization of mitochondrial membranes, occurring immediately following treatment of cells with PrP(106–126). Subsequently, cytochrome *c* was released and caspase-3 was activated. It has also been demonstrated that the fusogenic peptide PrP(118–135) induced time- and dose-dependent apoptosis in rat cortical and retinal neurons that included caspase-3 activation and DNA condensation/fragmentation [4,22]. These results have implicated mitochondria as the primary site of action [18]. Unfortunately, this implication has been restricted to the cell death with the artificial PrP peptides, and thereby further illustrates the significance of our current observations in terms of the neurotoxic property of wild-type PrP^C in vitro and in vivo.

There are potentially other mechanisms involved in neurotoxicity of the PrP^{Sc}-infected conditions, for example astrocytes, microglial cells and cytokines [17,25]. The activation of glial cells, which precedes neuronal death, and subsequent release of cytokines/chemokines may also contribute directly or indirectly to the neuronal cell death in prion diseases. In mutant PrP^C metabolism, on the other hand, the ER also seems to play another important role as well. Mutant PrP(Q217R) remains associated with the chaperone BiP at the ER for an abnormally long period of time and is degraded by the proteasomal pathway [11]. Nonetheless, our current observations suggest that wild-type PrP^C participate in the prion neurodegenerative cascade through the mitochondria-mediated events, at least in part. At the same time, the segregation of the infectious and neurotoxic properties of PrP suggests a new therapeutic strategy since prevention of mitochondrial mislocalization of PrP^C can be regarded as putative therapeutic targets aimed at protecting

cells from mitochondria-mediated apoptosis, even though the prion infection is not fully preventable.

Acknowledgements

We thank S.B. Prusiner for providing Tg(MoPrP)4053/FVB, T. Onodera for providing HpL3-4 cells, E. Nannri, K. Ishibashi, C. Ota, Y. Yamaura, and S. Wajima for technical assistance. We are indebted to G. Schatz, T. Omura, K. Mihara, R. Scheckman, and T. Momoi for helpful comments. This work was supported by grants from the Core Research for Evolutional Science and Technology (CREST) of the Japan Science and Technology Agency, Health and Labour Sciences Research Grants, Research on Advanced Medical Technology, nano-001, and the Ministry of Health, Labor and Welfare of Japan.

References

[1] Y. Bounhar, Y. Zhang, C.G. Goodyer, A. LeBlanc, Prion protein protects human neurons against Bax-mediated apoptosis, J. Biol. Chem. 276 (2001) 39145–39149.
[2] S. Brandner, S. Isenmann, A. Raeber, M. Fischer, A. Sailer, Y. Kobayashi, S. Marino, C. Weissmann, A. Aguzzi, Normal host prion protein necessary for scrapie-induced neurotoxicity, Nature 379 (1996) 339–343.
[3] N. Canu, C. Barbato, M.T. Ciotti, A. Serafino, L. Dus, P. Calissano, Proteasome involvement and accumulation of ubiquitinated proteins in cerebellar granule neurons undergoing apoptosis, J. Neurosci. 20 (2000) 589–599.
[4] J. Chabry, C. Ratsimanohatra, I. Sponne, P.P. Elena, J.P. Vincent, T. Pillot, In vivo and in vitro neurotoxicity of the human prion protein (PrP) fragment P118–135 independently of PrP expression, J. Neurosci. 23 (2003) 462–469.
[5] L.B. Chiarini, A.R. Freitas, S.M. Zanata, R.R. Brentani, V.R. Martins, R. Linden, Cellular prion protein transduces neuroprotective signals, EMBO J. 21 (2002) 3317–3326.
[6] R. Chiesa, D.A. Harris, Prion diseases: what is the neurotoxic molecule? Neurobiol. Dis. 8 (2001) 743–763.
[7] E. Cohen, A. Taraboulos, Scrapie-like prion protein accumulates in aggresomes of cyclosporin A-treated cells, EMBO J. 22 (2003) 404–417.
[8] B. Drisaldi, R.S. Stewart, C. Adles, L.R. Stewart, E. Quaglio, E. Biasini, L. Fioriti, R. Chiesa, D.A. Harris, Mutant PrP is delayed in its exit from the endoplasmic reticulum, but neither wild-type nor mutant PrP undergoes retrotranslocation prior to proteasomal degradation, J. Biol. Chem. 278 (2003) 21732–21743.
[9] M.E. Figueiredo-Pereira, K.A. Berg, S. Wilk, A new inhibitor of the chymotrypsin-like activity of the multicatalytic proteinase complex (20S proteasome) induces accumulation of ubiquitin-protein conjugates in a neuronal cell, J. Neurochem. 63 (1994) 1578–1581.
[10] G. Forloni, N. Angeretti, R. Chiesa, E. Monzani, M. Salmona, O. Bugiani, F. Tagliavini, Neurotoxicity of a prion protein fragment, Nature 362 (1993) 543–546.
[11] T. Jin, Y. Gu, G. Zanusso, M. Sy, A. Kumar, M. Cohen, P. Gambetti, N. Singh, The chaperone protein BiP binds to a mutant prion protein and mediates its degradation by the proteasome, J. Biol. Chem. 275 (2000) 38699–38704.
[12] R.R. Kopito, ER quality control: the cytoplasmic connection, Cell 88 (1997) 427–430.
[13] C. Kuwahara, A.M. Takeuchi, T. Nishimura, K. Haraguchi, A. Kubosaki, Y. Matsumoto, K. Saeki, T. Yokoyama, S. Itohara, T. Onodera, Prions prevent neuronal cell-line death, Nature 400 (1999) 225–226.
[14] J. Ma, S. Lindquist, Wild-type and PrP and a mutant associated with prion disease are subject to retrograde transport and proteasome degradation, Proc. Natl. Acad. Sci. U.S.A. 98 (2001) 14955–14960.
[15] J. Ma, R. Wollmann, S. Lindquist, Neurotoxicity and neurodegeneration when PrP accumulates in the cytosol, Science 298 (2002) 1781–1785.
[16] G. Mallucci, A. Dickinson, J. Linehan, P.C. Klohn, S. Brandner, J. Collinge, Depleting neuronal PrP in prion infection prevents disease and reverses spongiosis, Science 302 (2003) 871–874.
[17] M. Marella, J. Chabry, Neurons and astrocytes respond to prion infection by inducing microglia recruitment, J. Neurosci. 24 (2004) 620–627.
[18] C.N. O'Donovan, D. Tobin, T.G. Cotter, Prion protein fragment PrP-(106–126) induces apoptosis via mitochondrial disruption in human neuronal SH-SY5Y cells, J. Biol. Chem. 276 (2001) 43516–43523.
[19] E. Paitel, C. Alves da Costa, D. Vilette, J. Grassi, F. Checler, Overexpression of PrPc triggers caspase 3 activation: potentiation by proteasome inhibitors and blockade by anti-PrP antibodies, J. Neurochem. 83 (2002) 1208–1214.
[20] E. Paitel, R. Fahraeus, F. Checler, Cellular prion protein sensitizes neurons to apoptotic stimuli through Mdm2-regulated and p53-dependent caspase 3-like activation, J. Biol. Chem. 278 (2003) 10061–10066.
[21] V. Perrier, K. Kaneko, J. Safar, J. Vergara, P. Tremblay, S.J. DeArmond, F.E. Cohen, S.B. Prusiner, A.C. Wallace, Dominant-negative inhibition of prion replication in transgenic mice, Proc. Natl. Acad. Sci. U.S.A. 99 (2002) 13079–13084.
[22] T. Pillot, B. Drouet, M. Pincon-Raymond, J. Vandekerckhove, M. Rosseneu, J. Chambaz, A nonfibrillar form of the fusogenic prion protein fragment [118-135] induces apoptotic cell death in rat cortical neurons, J. Neurochem. 75 (2000) 2298–2308.
[23] R.K. Plemper, D.H. Wolf, Retrograde protein translocation: ERADication of secretory proteins in health and disease, Trends Biochem. Sci. 24 (1999) 266–270.
[24] S.B. Prusiner, Prions, Proc. Natl. Acad. Sci. U.S.A. 95 (1998) 13363–13383.
[25] J. Schultz, A. Schwarz, S. Neidhold, M. Burwinkel, C. Riemer, D. Simon, M. Kopf, M. Otto, M. Baier, Role of interleukin-1 in prion disease-associated astrocyte activation, Am. J. Pathol. 165 (2004) 671–678.
[26] L. Solforosi, J.R. Criado, D.B. McGavern, S. Wirz, M. Sanchez-Alavez, S. Sugama, L.A. DeGiorgio, B.T. Volpe, E. Wiseman, G. Abalos, E. Masliah, D. Gilden, M.B. Oldstone, B. Conti, R.A. Williamson, Cross-linking cellular prion protein triggers neuronal apoptosis in vivo, Science 303 (2004) 1514–1516.
[27] G.C. Telling, T. Haga, M. Torchia, P. Tremblay, S.J. DeArmond, S.B. Prusiner, Interactions between wild-type and mutant prion proteins modulate neurodegeneration in transgenic mice, Genes Dev. 10 (1996) 1736–1750.
[28] D. Westaway, J. Cayetano-Canlas, D. Groth, D. Foster, S.-L. Yang, M. Torchia, G.A. Carlson, S.B. Prusiner, Degeneration of skeletal muscle, peripheral nerves, and the central nervous system in transgenic mice overexpressing wild-type prion proteins, Cell 76 (1994) 117–129.
[29] Y. Yedidia, L. Horonchik, S. Tzaban, A. Yanai, A. Taraboulos, Proteasomes and ubiquitin are involved in the turnover of the wild-type prion protein, EMBO J 20 (2001) 5383–5391.
[30] G. Zanusso, R.B. Petersen, T. Jin., Y. Jing, R. Kanoush, S. Ferrari, P. Gambetti, N. Singh, Proteasomal degradation and N-terminal protease resistance of the codon 145 mutant prion protein, J. Biol. Chem. 274 (1999) 23396–23404.
[31] H. Zhou, F. Cao, Z. Wang, Z.X. Yu, H.P. Nguyen, J. Evans, S.H. Li, X.J. Li, Huntingtin forms toxic NH_2-terminal fragment complexes that are promoted by the age-dependent decrease in proteasome activity, J. Cell Biol. 163 (2003) 109–118.

BIOLOGY OF REPRODUCTION 73, 29–35 (2005)
Published online before print 2 March 2005.
DOI 10.1095/biolreprod.104.037077

Ubiquitin C-Terminal Hydrolase L-1 Is Essential for the Early Apoptotic Wave of Germinal Cells and for Sperm Quality Control During Spermatogenesis[1]

Jungkee Kwon,[3,4] Keiji Mochida,[5] Yu-Lai Wang,[3] Satoshi Sekiguchi,[4] Tadashi Sankai,[6] Shunsuke Aoki,[3] Atsuo Ogura,[5] Yasuhiro Yoshikawa,[4] and Keiji Wada[2,3]

Department of Degenerative Neurological Disease,[3] National Institute of Neuroscience, National Center of Neurology and Psychiatry, Kodaira, Tokyo 187-8502, Japan
Department of Biomedical Science,[4] Graduate School of Agricultural and Life Sciences, University of Tokyo, Bunkyo-ku, Tokyo 113-8657, Japan
Bioresource Engineering Division,[5] Bioresource Center, Riken, Tsukuba, Ibaraki 305-0074, Japan
Tsukuba Primate Center,[6] National Institute of Infectious Diseases, Tsukuba, Ibaraki 305-0843, Japan

ABSTRACT

Ubiquitination is required throughout all developmental stages of mammalian spermatogenesis. Ubiquitin C-terminal hydrolase (UCH) L1 is thought to associate with monoubiquitin to control ubiquitin levels. Previously, we found that UCHL1-deficient testes of *gad* mice have reduced ubiquitin levels and are resistant to cryptorchid stress-related injury. Here, we analyzed the function of UCHL1 during the first round of spermatogenesis and during sperm maturation, both of which are known to require ubiquitin-mediated proteolysis. Testicular germ cells in the immature testes of *gad* mice were resistant to the early apoptotic wave that occurs during the first round of spermatogenesis. TUNEL staining and cell quantitation demonstrated decreased germ cell apoptosis and increased numbers of premeiotic germ cells in *gad* mice between Postnatal Days 7 and 14. Expression of the apoptotic proteins TRP53, Bax, and caspase-3 was also significantly lower in the immature testes of *gad* mice. In adult *gad* mice, cauda epididymidis weight, sperm number in the epididymis, and sperm motility were reduced. Moreover, the number of defective spermatozoa was significantly increased; however, complete infertility was not detected. These data indicate that UCHL1 is required for normal spermatogenesis and sperm quality control and demonstrate the importance of UCHL1-dependent apoptosis in spermatogonial cell and sperm maturation.

apoptosis, early apoptotic wave, epididymis, gad *mouse, sperm, spermatogenesis, sperm quality, testis, UCHL1*

INTRODUCTION

Ubiquitin and ubiquitin-dependent proteolysis are involved in a variety of cellular processes, such as cell cycle progression, degradation of intracellular proteins, programmed cell death, and membrane receptor endocytosis [1–5]. In spermatogenesis, the ubiquitin-proteasome system is required for the degradation of numerous proteins throughout the mitotic, meiotic, and postmeiotic developmental phases [4, 6, 7]. Ubiquitin C-terminal hydrolases (UCHs) control the cellular ubiquitin balance by releasing ubiquitin from tandemly conjugated ubiquitin monomers (*Ubb, Ubc*) and small adducts or unfolded polypeptides [4, 8–10]. UCHL1 is expressed at high levels in both testis and epididymis and may play an important role in the regulation of spermatogenesis [11–14]. In addition to its hydrolase activity [15], UCHL1 has a variety of functions, including dimerization-dependent ubiquityl ligase activity, and association with and stabilization of monoubiquitin in neuronal cells [16–18]. Furthermore, it has been suggested that UCHL1 also functions as a regulator of apoptosis [19]. The gracile axonal dystrophy (*gad*) mouse is an autosomal recessive spontaneous mutant carrying an intragenic deletion of the gene encoding *Uchl1* [21]. We recently found that testes of *gad* mice, which lack UCHL1 expression [18, 20, 21], have reduced ubiquitin levels and are resistant to cryptorchid injury-mediated germ cell apoptosis [22].

During prepubertal development, an early and massive wave of germinal cell apoptosis occurs in mouse testis [23, 24]. This early germ cell apoptotic wave affects mainly spermatogonia and spermatocytes and appears to be essential for functional spermatogenesis in adulthood. Decreased apoptosis has been reported in the early phase of spermatogenesis in transgenic mice overexpressing the antiapoptotic proteins *Bcl2* or *Bcl-xL* [23, 25] and in mice deficient in the apoptotic protein *Bax* [26]. This reduction in apoptosis is associated with the disruption of normal spermatogenesis and infertility. Our previous work demonstrated that *gad* mice exhibit pathological changes such as progressively decreasing spermatogonial stem cell proliferation [13] and increased expression of the antiapoptotic proteins Bcl2 and Bcl-xL in response to apoptotic stress [19, 22]. Furthermore, we showed that UCHL1 functions during prepubertal development to effect normal spermatogenesis and to modulates germ cell apoptosis [22]. However, the mechanism by which UCHL1 regulates apoptosis during prepubertal development remains unclear. To further investigate the role of UCHL1 in immature testes, we evaluated the function of UCHL1 during early spermatogenesis. Here, we show that immature testes of *gad* mice accumulate premeiotic germ cells and are resistant to the massive wave of germinal cell apoptosis during the first round of spermatogenesis, eventually leading to alterations in sperm produc-

[1]Supported by Grants-in-Aid for Scientific Research from the Ministry of Health, Labour and Welfare of Japan; Grants-in-Aid for Scientific Research from the Ministry of Education, Culture, Sports, Science and Technology of Japan; a grant from the Pharmaceuticals and Medical Devices Agency of Japan; and a grant from Japan Science and Technology Agency.
[2]Correspondence: Keiji Wada, Department of Degenerative Neurological Disease, National Institute of Neuroscience, National Center of Neurology and Psychiatry, Kodaira, Tokyo 187-8502, Japan.
FAX: 81 42 341 1745; e-mail: wada@ncnp.go.jp

Received: 16 October 2004.
First decision: 16 December 2004.
Accepted: 21 February 2005.

ISSN: 0006-3363. http://www.biolreprod.org

tion, motility, and morphology in adult mice. Our data suggest that UCHL1-dependent apoptosis is essential for normal spermatogenesis.

MATERIALS AND METHODS

Animals

We used male *gad* (CBA/RFM) mice [21] at 7, 14, 21, 28, and 35 days and 10 wk of age. The *gad* mouse is an autosomal-recessive mutant that was produced by crossing CBA and RFM mice. The *gad* line was maintained by intercrossing for more than 20 generations. This strain was maintained at our institute. Animal care and handling were in accordance with institutional regulations and were approved by the Animal Investigation Committee of the National Institute of Neuroscience, National Center of Neurology and Psychiatry.

Histological and Immunohistochemical Assessment of Testes

Testes were embedded in paraffin wax after fixation in 4% paraformaldehyde, sectioned at 4-μm thickness, and stained with hematoxylin for counting [13]. Light microscopy was used for routine observations. For immunohistochemical staining, the sections were incubated with 10% goat serum for 1 h at room temperature followed by incubation overnight at 4°C with a rabbit polyclonal antibody against UCHL1 (1:1000 dilution; peptide antibody) [20] in PBS containing 1% BSA. Sections were then incubated for 1 h with biotin-conjugated anti-rabbit IgG diluted 1:200 in PBS, followed by Vectorstain ABC-PO (Vector Laboratories, Burlingame, CA) for 30 min at room temperature. Sections were developed using 3,3′-diaminobenzidine and counterstained with hematoxylin.

Apoptotic cells in testicular tissues were identified by terminal deoxynucleotidyl transferase (TdT)-mediated nick end labeling (TUNEL) using the DeadEnd Fluorometric TUNEL system (Promega, Madison, WI) according to the manufacturer's instructions.

Quantitative Analysis of Testicular Cell Number

The total number of cells was determined by counting the testicular cells including Sertoli cells of seminiferous tubules. Quantitative determinations were made using four each of wild-type and *gad* mice at 7 and 14 days of age. Five sections from each mouse were processed in parallel for counterstaining with hematoxylin. Twenty circular seminiferous tubules in each section were then selected by randomly from those tubules, and 400 circular seminiferous tubules were measured using the 400× lens of a Zeiss Axioplan microscope. The total cell number was not determined by dividing cell types such as testicular germ cells and Sertoli cells because it was difficult to determine the difference of cell types [26]. There were no significant differences in nuclear size in either of the group studies. Thus, the total number of cells reflected all cell types of seminiferous tubules.

Quantitative Analysis of Apoptotic Germ Cells

Quantification was performed using four each of wild-type and *gad* mice at 7, 14, 21, 28, and 35 days of age. The total number of apoptotic cells was determined by counting the positively stained nuclei in 20 circular seminiferous tubules in each section [22]. Five sections from each mouse and a total 400 circular seminiferous tubules per each group were processed.

Germ Cell Isolation, Culture, and Viability Measurement

Germ cells from wild-type and *gad* mice were prepared using a modification of the procedure described by Kwon et al. [20]. Briefly, testes from three 2-wk-old mice were incubated twice for 30 min at 25°C in Dulbecco Modified Eagle medium (DMEM)-F12 medium containing 0.5 mg/ml collagenase IV-S (Sigma-Aldrich, St. Louis, MO) and then digested for 60 min at 25°C in DMEM-F12 medium containing 1 mg/ml trypsin (Sigma-Aldrich). The cell suspension was digested and washed several times to eliminate testicular somatic cells. The cells were then counted and cultured at 2.0×10^5 cells/ml in DMEM-F12 medium containing 10% fetal bovine serum (FBS). The cells were harvested at each day for 5 days, and viability was assessed using the Vi-Cell XR cell viability analyzer (Beckman Coulter, Fullerton, CA).

Quantitative mRNA Analysis of Uchl1 and Uchl3 Genes by Real-Time PCR

SYBR Green-based real-time quantitative reverse transcription-polymerase chain reaction (RT-PCR; PRISM 7700 Sequence detection system, ABI, Columbia, MD) was performed [20] in SYBR Green Master mix using the following primers: *Uchl1*, 5′-TTCTGTTCAACAACGTGGACG-3′ and 5′-TCACTGGAAAGGGCATTCG-3′; *Uchl3*, 5′-TGAAGGTCAGACTGAGGCACC-3′ and 5′-AATTGGAAATGGTTTCCGTCC-3′; β-actin, 5′-CGTGCGTGACATCAAAGAGAA-3′ and 5′-CAATAGTGATGACCTGGCCGT-3′ To compare *Uchl1* and *Uchl3* gene expression in the first round of spermatogenesis, the formula 2^{-ddCt} was used to calculate relative expression compared with testes of 7-day-old mice.

Western Blotting

Western blots were performed as previously reported [19, 22]. Total protein (5 μg/lane) was subjected to SDS-polyacrylamide gel electrophoresis using 15% gels (Perfect NT Gel, DRC, Japan). Proteins were electrophoretically transferred to polyvinylidene difluoride membranes (Bio-Rad, Hercules, CA) and blocked with 5% nonfat milk in TBS-T (50 mM Tris base, pH 7.5, 150 mM NaCl, 0.1% [w/v] Tween-20). The membranes were incubated individually with one or more primary antibodies to UCHL1 and UCHL3 (1:1000 dilution; peptide antibodies) [20], Bcl-xL, Bax, TRP53, and inactive caspase-3 (1:1000 dilution; all from Cell Signaling Technology, Beverly, MA). Blots were further incubated with peroxidase-conjugated goat anti-mouse IgG or goat anti-rabbit IgG (1:5000 dilution; Pierce, Rockford, IL) for 1 h at room temperature. Immunoreactions were visualized using the SuperSignal West Dura Extended Duration Substrate (Pierce) and analyzed using a ChemiImager (Alpha Innotech, San Leandro, CA).

Sperm Motility, Morphology, and Immunohistochemical Assessments

Sperm were collected from the right cauda epididymidis [27] of 10-wk-old wild-type and *gad* mice in 400 μl human tubal fluid medium containing 0.5% bovine serum albumin and then incubated at 37°C under 5% CO_2 in air for 1–2 h. Using a computer-assisted semen analysis system (TOX IVOS, Hamilton Throne Research, Beverly, MA) [28], sperm were analyzed for the following motion parameters: percentage of motile sperm (MSP), percentage of progressively motile sperm (PMP), average path velocity (VAP), straight-line velocity (VSL), curvilinear velocity (VCL), lateral head displacement (ALH), linearity (VSL/VCL × 100), and straightness (VSL/VAP × 100). All procedures were performed at 37°C. To study the spermatozoa morphology, sperm were smeared and then evaluated for defects in the head, midpiece, and principal piece and for head detachment. For immunocytochemical staining, the sections were incubated with antibodies against UCHL1 (1:1000 dilution; peptide antibody) [20] and ubiquitin (1:500 dilution; DakoCytomation, Glostrup, Denmark) overnight at 4°C in PBS containing 1% BSA.

Statistical Analysis

The mean and standard deviation were calculated for all data (presented as mean ± SD). One-way analysis of variance (ANOVA) was used for all statistical analyses.

RESULTS

Expression of UCHL1 During the First Round of Spermatogenesis

We used Western blotting to characterize the level of UCHL1 and UCHL3 expression in testes from immature wild-type and *gad* mice (Fig. 1, B and C). In agreement with previous data [20], UCHL1 expression was significantly elevated on Day 14 in testicular lysates obtained from 7-, 14-, 21-, 28-, and 35-day-old wild-type mice. The level of UCHL3 expression increased with age and did not differ between *gad* and wild-type mice (Fig. 1B), suggesting that UCHL3 expression is regulated independently of UCH-L1 during the first round of spermatogenesis [20]. We also assessed the expression pattern of *Uchl1* and *Uchl3* genes during juvenile spermatogenesis using SYBR Green-